CROSS SECTIONS FOR CHARGE TRANSFER BETWEEN MERCURY IONS AND OTHER METALS

FINAL REPORT

David A. Vroom
John A. Rutherford

Prepared for
NATIONAL AERONAUTICS AND SPACE ADMINISTRATION
NASA Lewis Research Center
Under
Contract NAS 3-17759
William R. Kerslake, Program Manager

June 16, 1977

1. Report No.	2. Government Accession No.	3. Recipient's Catalog No.
NASA CR-135205		

4. Title and Subtitle	5. Report Date
CROSS SECTIONS FOR CHARGE TRANSFER BETWEEN MERCURY IONS AND OTHER METALS	June 16, 1977
	6. Performing Organization Code

7. Author(s)	8. Performing Organization Report No.
David A. Vroom John A. Rutherford	8095-046
	10. Work Unit No.

9. Performing Organization Name and Address	11. Contract or Grant No.
IRT Corporation P. O. Box 80817 San Diego, CA 92138	NAS 3-17759
	13. Type of Report and Period Covered FINAL June 1973-April 1977

12. Sponsoring Agency Name and Address	14. Sponsoring Agency Code
National Aeronautics and Space Administration Lewis Research Center 21000 Brookpark Road, Cleveland, OH 44135	

15. Supplementary Notes

Project Manager: William R. Kerslake, NASA Lewis Research Center, Cleveland, Ohio

16. Abstract

Cross sections for charge transfer between several ions and metals of interest to the NASA electro-propulsion program have been measured. Specifically, the ions considered were Hg^+, Xe^+ and Cs^+ and the metals Mo, Fe, Al, Ti, Ta, and C. Measurements were made in the energy regime from 1 to 5000 eV. In general, the cross sections for charge transfer were found to be less than 10^{-15} cm^2 for most processes over the total energy range. Exceptions are Hg^+ in collision with Ti and Ta. The results obtained for each reaction are given in both graphical and numerical form in the text. For quick reference, the data at several ion velocities, is condensed into one table given in the summary.

17. Key Words (Suggested by Author(s))	18. Distribution Statement
Electric propulsion Mercury propellant Xenon propellant Cesium propellant Charge transfer	UNCLASSIFIED — Unlimited

19. Security Classif. (of this report)	20. Security Classif. (of this page)	21. No. of Pages	22. Price*
Unclassified	Unclassified	53	

* For sale by the National Technical Information Service, Springfield, Virginia 22151

NASA-C-168 (Rev. 6-71)

CONTENTS

FIGURES

TABLES

1. INTRODUCTION

This report summarizes data obtained for the National Aeronautics and Space Administration, Lewis Research Center under Contract NAS 3-17759. The data obtained is of direct relevance to a current NASA need.

In the operation of electro-propulsion engines, a long-term problem may arise if low-vapor pressure metal emitted from the thruster plated out on other components of the spacecraft. In particular, the plating out of metals on the solar panels generating the power for the thruster would be detrimental to extended operation (Ref. 1).

The main objective of the program was to obtain information needed to determine if this plating is a serious problem. The source of these metals is the erosion of metallic atoms from the grids and support structures of the device. This erosion can arise from several processes such as sputtering due to bombardment of the ions used in the engine on these thruster components. If these sputtered neutrals are to be a problem, they must charge-transfer with the thruster ions, and the charge particles drift out of the ion beam and impinge on other vehicle components. The sputtering is known to occur, but to determine if a problem exists, the charge-transfer cross sections between ions such as Hg^+, Xe^+ and Cs^+, and neutral atoms such as Mo, Fe, Al, Ti, C and Ta must be measured. The actual processes considered here can be represented as

$$Hg^+ + Mo \rightarrow Hg + Mo^+ \quad (1)$$

$$Xe^+ + Mo \rightarrow Xe + Mo^+ \quad (2)$$

$$Hg^+ + Fe \rightarrow Hg + Fe^+ \quad (3)$$

$$Xe^+ + Fe \rightarrow Xe + Fe^+ \quad (4)$$

$$Cs^+ + Fe \rightarrow Cs + Fe^+ \quad (5)$$

$$Hg^+ + Al \rightarrow Hg + Al^+ \quad (6)$$

$$Xe^+ + Al \rightarrow Xe + Al^+ \quad (7)$$

$$Cs^+ + Al \rightarrow Cs + Al^+ \quad (8)$$

$$Hg^+ + Ti \rightarrow Hg + Ti^+ \quad (9)$$

$$Xe^+ + Ti \rightarrow Xe + Ti^+ \quad (10)$$

$$Hg^+ + Ta \rightarrow Hg + Ta^+ \quad (11)$$

$$Hg^+ + C \rightarrow Hg + C^+ \quad (12)$$

$$Hg^+ + C_2 \rightarrow Hg + C_2^+ \quad (13)$$

$$Hg^+ + C_3 \rightarrow Hg + C_3^+ \quad (14)$$

The main purpose of the program was to measure cross sections for these processes. The ion energy range of the experiments was 1 to 5000 eV.

A secondary purpose was to determine if the charge-transfer process gives rise to any optical emissions. These emissions could then be used as signatures for these charge transfer processes occurring within the thruster.

The experimental technique used in the study of charge transfer was crossed-ion and modulated neutral beams. The instrument used, which has been fully described in journal publications (Ref. 2,3,4) was initially developed some years ago and has undergone continuous improvement since that time such that it is now reliable and highly refined. The versatility of this instrument makes it ideal for the study of many reactions involving charged and neutral species. Of special importance is the fact that the neutrals can be formed as a beam in a separate section of the apparatus, thereby allowing labile species to be studied.

The optical studies were performed using a modulated ion beam crossing a neutral quasi beam of the desired metal. This apparatus, which was assembled for the study reported here, is in many ways similar to the instrument used for the charge transfer measurements.

The following sections of this report describe the apparatus used for the experimental measurements, the special furnaces constructed to produce the neutral beams of metal atoms, the results of the measurements and the interpretation of the results.

2. EXPERIMENTAL METHODS

The crossed ion-modulated neutral beam apparatus has been described in the literature (Refs. 2,3,4). For completeness, however, a further description is given here. The methods employed in forming the ion beams of xenon, mercury, and cesium, as well as the neutral beams of the various metals studied, will be discussed. A description of the apparatus used for the optical studies will be given. Also included will be a discussion of how the density of the metal atoms in the neutral beam is obtained.

2.1 THE CROSSED ION-MODULATED NEUTRAL BEAM APPARATUS

2.1.1 Primary and Secondary Ion Systems

Figure 1 shows a schematic of the experimental apparatus. The primary ions are extracted from the source and mass-analyzed at an energy of 75 eV in a 180° magnetic mass spectrometer. After analysis, the ions pass through an aperture in an iron plate that shields the magnetic field of the mass analyzer from the succeeding regions of the apparatus. The ions are then retarded or accelerated to the desired collision energy, and pass through a field-free region before intersecting the neutral beam. Collimating apertures ensure that, from purely geometric considerations, all primary ions pass through the modulated neutral beam. The neutral beam is modulated at 100 Hz by mechanical chopping.

Secondary ions resulting from collisions between the primary ions and neutral species are extracted along the direction of the primary ion beam by an electric field of approximately 2 V/cm. These ions then enter an electric field in which their energy is increased to 1650 eV. Penetration of this accelerating field into the interaction region is reduced by the use of a double-grid structure.

After acceleration, the ions pass through an electrostatic quadrupole lens that forms the entrance slit for a 60°-sector magnetic mass spectrometer. The mass-selected ions impinge on the first dynode of a 14-stage CuBe electron multiplier. For all ions formed by charge transfer or ion-molecule reactions,

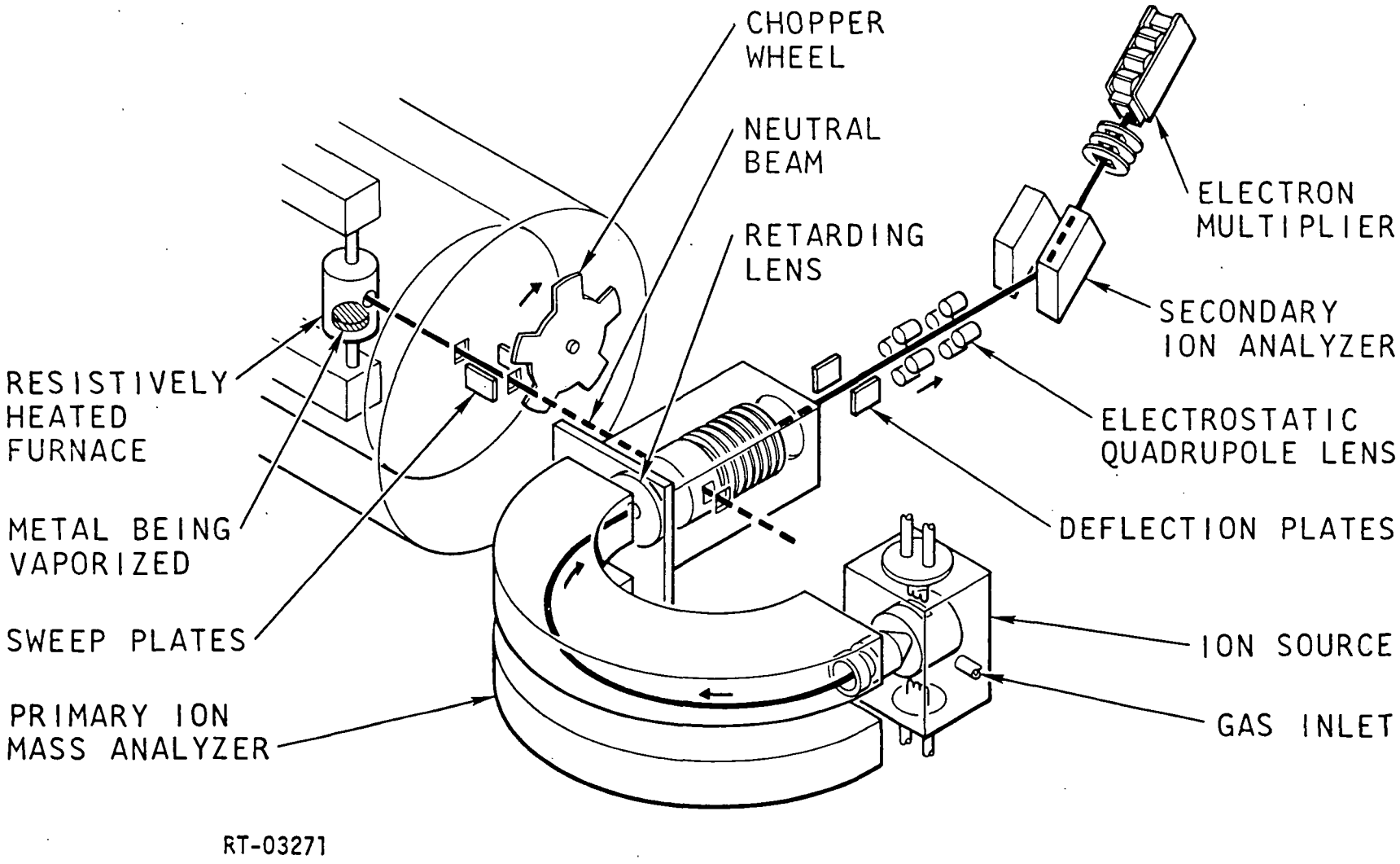

Figure 1. Crossed-ion and neutral-beam apparatus

the most abundant isotope is used when making measurements. The cross sections are corrected for the isotope effect created by collecting only those having this mass. The output from the multiplier passes successively through a pre-amplifier, 100-Hz narrow-band amplifier, and a phase-sensitive detector, and is then integrated. The output is presented on a chart recorder.

The primary ion-beam intensity is measured at the interaction region with a Faraday cup, which can be moved into the collision region when desired. The primary ion energy is determined from retarding potential measurements. All surfaces at the interaction region are gold plated and the Faraday cup is coated with alkadag,* and the interaction region is normally maintained at 120°C to minimize surface charging.

Because in the proposed work the energy range extends to low collision energies, only weak extraction fields at the collision region will be used. As a result, the secondary ions will not be collected with 100% efficiency. Obtaining absolute cross sections for production of various secondary ions requires, therefore, determination of the overall detection efficiency. This latter consideration is governed by a number of factors, including the multiplier gain and the efficiency of transmission of the secondary ions from the interaction region to the multiplier.

The multiplier-amplifier-recorder gain is measured by modulating the primary ions prior to their entry into the collision region. The ion current signal is first measured with the movable Faraday cup and, after traversing the secondary mass spectrometer multiplier-amplifier system, by the recorder. Primary ion transmission through the second mass spectrometer is 92%. Typical gains for the entire system are of the order of 10^{15} output volts on the recorder per ampere of incoming current. In practice, gains are measured for each product ion.

The major experimental uncertainty is associated with the collection of efficiency for the secondary ions at low energies. Collection fields large enough to ensure total collection of the secondary ions cannot be used here because of the influence these fields exert on the motion of low-energy primary ions. In general, the collection efficiency obtained in the low energy regime is of the order of 75% but varies somewhat for different processes.

Estimates of the collection efficiency obtained at low ion energies can be made by going to higher ion energies and applying sufficiently strong extraction

*A colloidal solution of graphite in alcohol.

fields to obtain total ion collection. Comparison of the signals with saturated and "normal" extraction fields yields the collection efficiency. This test can only be performed at ion energies high enough such that the perturbation of the primary ion energy by the extraction field is small. The results are not necessary relevant to the low-energy regime, where the dynamics of the ion-neutral process may be different. Interpretation of data obtained using different collection fields is based on the assumption that, for primary ion energies above approximately 10 eV, the secondary ions are collected with nearly equal efficiency, and that, as a result, the collection efficiency is independent of both the nature and the energy of the primary ions. This assumption implies that the energy defect in the reaction is not large, since energy not expended in excitation of the products must appear as kinetic energy and, therefore, would influence the collection efficiency.

2.1.2 The Ion Sources

Both mercury and xenon ions were formed by electron bombardment in a conventional low pressure ion source. The pressure in this source is generally of the order of one millitorr during operation and no discharge is struck. The ions are formed by electron impact in a field free region, and extracted uniformly for injection into the magnetic field of the first mass spectrometer. The result is that the energy spread of the ions is small; a necessary condition if one is to study processes at very low ion energies. Currents of 10^{-9}A of ions can readily be formed using this source.

The cesium ions used in these experiments were formed by surface ionization. The technique employed is as follows. A filament of tungsten stocking mesh is dipped in an aqueous solution of Cs_2SO_4 and allowed to dry in air. This filament is then installed in our source such that the mesh is near the exit hole. Heating of the mesh to 1600 K leads to emission of copious quantities of Cs^+ ions. The use of Cs_2SO_4 as a surface ionization source of Cs^+ has been described previously (Ref. 5).

2.1.3 Neutral Beam Formation and Density Measurement

The method used to form the metal vapor necessary for beam formation depended on the metal being studied. The various techniques employed will be discussed in detail in the following section.

After formation, the metal atoms effuse from one chamber of the vacuum system through an intermediate chamber and into the main collision region (see Figure 1). Slits in the vacuum walls between these sections serve to collimate the atom beam. Sweep plates in the central chamber are used to eliminate any charge particles

which may be present. Just before the neutral particles intersect the ion beam, they are mechanically chopped at 100 Hz, thereby allowing modulated beam techniques to be employed for detection of the secondary ions.

We commonly use one of two techniques to determine the neutral beam density in our experiments. The first uses the cosine law for molecular effusion (Ref. 6). Here it is necessary to know the temperature and pressure in the source, the area of the aperture leading from the source into the vacuum and the distance from the source to the interaction region. For metals this technique can be employed if the material has a vapor pressure such that it can be heated in an enclosed crucible to temperatures high enough to generate a pressure sufficient to give a usable beam density ($\sim$ 10 to 100 millitorr). In addition the metal must not react with the walls of the container at high temperature. If these conditions are met, then using the vapor pressure tables of Honig (Ref. 7), it is possible to calculate the neutral beam density in the interaction region. A more extensive discussion on the determination of the beam density in this manner is given in Reference 2.

The second method used to determine the neutral beam density of condensible materials, such as metal vapors, is neutron activation analysis. We have employed this technique previously to determine metal atom beam densities, and a description of the technique appears in Reference 2. Briefly, the neutral beam is run under constant conditions for several hours and all the metal passing through the collision region is collected in a specially prepared polyethylene container. During the time the beam is running, the signal for a reference reaction and all other relevant instrument parameters are recorded. After collection of the beam, the polyethylene container is removed from the apparatus and sent to a neutron activation analysis facility so that the amount of metal collected can be determined. Quantities of the order of 1×10^{-6} grams are routinely determined with an accuracy of $\pm$10%. Using the measured amount collected in the container and the time that the neutral beam was run, the beam density can be determined. Typical beam densities were of the order of 4×10^{8} particles/cm^3. Knowing the beam density, the signal for the reference reaction, and the primary ion beam current, the cross section for the reference reaction can be determined.

2.2 FURNACE DESIGNS

With nearly every metal studied under this contract, it was necessary to develop a new type of furnace in order to produce sufficient quantities of the neutral particle. The various designs are detailed below.

2.2.1 The Iron Atom Source

The furnace used to produce iron atoms has been described previously in the literature (Ref. 8). The low vapor pressure of iron required an effusion source capable of withstanding high temperatures ($\sim 1800^{\circ}K$). Further, it was necessary to use an inert material since iron is very reactive at the temperatures required. The cell used was constructed from a high purity alumina crucible surrounded by tungsten foil. The location of the crucible is given in Figure 1. The crucible and foil are held in position by tantalum endcaps held between two bus bars. Passage of current through the foil served to heat the crucible. The temperature was monitored using an optical pyrometer. Pure iron wire placed in the crucible served as the source of iron vapor. Pressures of the order of 50 millitorr were generally used in the crucible. The neutral beam was formed by effusion of the iron vapor from a small hole in the side of the crucible. At the pressures used in the metal vapor cell, dimerization is not expected to be a problem but in spite of this, during the course of the experiments, attempts were made to see charge transfers to polymers in the beam. No evidence of such species was found.

The iron source operated as a Knudsen cell and as a consequence it was possible to determine the neutral beam density using both calculation and direct measurement (activation analysis). The two methods gave results that agreed to within 10%.

2.2.2 The Molybdenum Source

Two sources were employed successfully to form a beam of neutral molybdenum atoms. The first method was free evaporation of particles directly from a resistively heated pure molybdenum tube and the second was evaporation of the metal from a tantalum crucible. Both methods gave similar results.

The first source consisted of a piece of thin walled molybdenum tubing held between the two stainless steel bus bars shown in Figure 1. The tube was

0.125 in. O.D. with a wall thickness of 0.011 in. and was 3 inches long. Water cooling in the bus bars was used for cooling the ends of the tube, the center of which was heated by passage of 150 amps of current. The temperature uniformity of the center of the tube was increased by using two tantalum heat shields. Use of these shields also lowered the power required for heating. Holes in the heat shields served as the first collimation apertures for the Mo beam.

A problem was encountered with this free evaporation source that appeared to result from carbon impurity in the metal. On initial heating a carbide layer appeared to form on the surface which inhibited the free evaporation of the metal. Experimentally it was found that flashing the tube to a temperature above that which should be required to give a usable beam drove off this surface layer and upon cooling a stable beam was obtained. A typical beam density was $1 \times 10^8/cm^3$.

Even though satisfactory results could be obtained by free evaporation of Mo atoms from a tube of the material, the short life time (5-8 hours) of these sources made measurement tedious. This problem prompted us to try a different furnace arrangement. In this new design a thin walled tantalum tube is used. It is positioned between the two bus bars shown in Figure 1. A small amount of pure molybdenum is enclosed in the central section of this tube by two tantalum plugs which are pushed in from either end. A small exit hole in the tube (approximately 1 mm) serves to let the molybdenum vapor escape. This arrangement approximates a Knudsen cell and as a consequence a calculation can be used to determine the beam flux from the furnace provided no reaction occurs between the tantalum and the molybdenum.

This new type of furnace, which is similar to ones we have employed previously (Ref. 2), has a much longer lifetime than the tubes used previously if the temperature of the tantalum is kept below 2800 K. This temperature is significant for two reasons. First, it is just below the melting point of molybdenum and no reaction appears to occur between the two metals (examination of a furnace after several hours of operation showed the molybdenum still present in free form) and, second, this is the highest temperature to which a tantalum furnace can safetly be heated without seriously decreasing its lifetime.

Use of this new design of furnace has provided a check on our beam density measurements. The cross sections for charge transfer to molybdenum determined

using a beam density obtained from neutron activation analysis, and a beam density calculated assuming the tantalum crucible operates as a Knudsen cell, agreed to within 30%.

A disagreement of 30% is much larger than we have routinely encountered in comparison of Knudsen cell and activation analysis results. In this case, we feel that the difference probably arises because the tantalum furnace containing the molybdenum probably did not operate as a true Knudsen cell due to reaction between the metals. The beam densities obtained using neutron activation analysis were used in calculating the cross sections.

The beam density from the new source was very similar to that obtained using free evaporation but the lifetime of the tantalum source was considerably longer.

2.2.3 The Aluminum Source

The aluminum neutral beam was produced by heating the pure metal in a boron nitride crucible. The actual source was identical to the iron atom source described in Section 2.2.1 with the exception that the alumina was replaced by boron nitride. This furnace was very reliable and operated as a true Knudsen cell thereby allowing the beam density to be calculated using our standard techniques. The Knudsen cell characteristics of our crucible were fortunate since neutron activation analysis could not be used in the case of aluminum. This occurred not because aluminum cannot be detected by neutron activation analysis but rather because aluminum is ubiquitous in nature and it was impossible to collect a sample which was not highly contaminated.

Operation of the aluminum furnace resulted in our obtaining considerable experience in working with this metal. In order to obtain a pure Al atom beam the following precautions were taken for each new furnace loading. First, before loading, the boron nitride was outgassed at elevated temperatures to drive out all contaminants which could react with the hot metal. Second, the aluminum metal used was of very high purity. Further, it was necessary to keep a good vacuum over the metal during and after its initial heating since any oxygen which is present leads to formation of Al_2O_3. The presence of any of this oxide prevents the evolution of pure aluminum. This arises because Al_2O_3 decomposes when heated in the presence of metallic aluminum to form a lower oxide (Ref. 9).

$$Al_2O_3 + 4Al \rightarrow 3Al_2O \quad . \tag{15}$$

In our initial heating of a furnace freshly loaded with pure aluminum (which is always covered by a thin coat of Al_2O_3), we observed the evolution of Al_2O indicating that reaction (15) was occurring. Further, no Al atoms were evolved until

all the Al_2O_3 had been converted to Al_2O and expelled.

2.2.4 The Titanium Source

The source used for the titanium measurements was the same as the second of the two methods described for molybdenum in Section 2.2.2. That is, pure titanium metal was held in the center portion of a tantalum tube furnace by two tantalum plugs. These plugs were inserted from either end of the furnace tube and swaged into position. Titanium vapor escapes through a small hole in the side of the furnace which is held between the two bus bars shown in Figure 1. As was the case with molybdenum, the tube was heated by the passage of current and surrounded by heat shield to minimize heat losses.

Although the tantalum furnace was adequate for our measurements, it never operated in a completely satisfactory manner. The major problems were that the beam density appeared to vary in a pulsed fashion and there also appeared to be other materials present. In order to better understand the operation of this source a study was conducted using another source, namely, a graphite crucible. The graphite crucible was found to operate much as the tantalum furnace had and we therefore concluded that the problem was not associated with the furnace materials. A series of careful tests of furnace operation (stability of the beam, and appearance of possible contaminants) were conducted as a function of furnace temperature. From this it was concluded that the major difficulty we had been experiencing was coming from operating the furnace too hot. That is, where the vapor pressure of the Ti was too high for effective Knudsen cell operation. The high vapor pressure resulted in the unstable beam and in the appearance of unknown mass peaks in the mass spectrum. The appearance of the extra mass peaks is not fully understood but may be related to the presence of dimers in the high pressure neutral beam. The implication of these tests is that the vapor pressure of Ti as listed in the literature (Ref. 7) may be incorrect.

2.2.5 The Tantalum Source

In order to form a beam of tantalum neutral particles of sufficient intensity to allow measurement of charge transfer cross sections, it was necessary to use temperatures in excess of what any conceivable crucible material could withstand. For this reason it was necessary to go to electron beam heating of a small sample of the material supported by a thin rod of low vapor pressure metal. In this case the rod was also made of tantalum.

The e-gun heater had to be built completely in our laboratory since no commercial models were small enough to fit into the restricted beam source area of our apparatus.

The heater which is shown schematically in Figure 2, consists basically of a filament, accelerating plates, and a magnetic field for bending the electrons around onto the sample. The magnetic field is supplied by two specially shaped pole pieces onto which a permanent magnet is attached. The pole pieces and the filament assembly are mounted on a water cooled copper base plate. This base plate was bolted to a support rod which was in fact one of the bus bars of our normal furnace holder shown in Figure 1. The e-gun is designed to work with currents up to 50 mA and an energy of approximately 5 kV.

The major difficulty in using the e-gun heater to form a neutral beam of low vapor pressure materials was that an irreducible background signal was created by the electron beam colliding with the target material. Tests indicated that the source of this background was probably soft x-rays emitted by the target material which passed into the collision region where they ionized the background gas and neutral beam particles.

The e-beam heater was found to give stable beams of Ta of sufficient intensity that measurements could be made in spite of the presence of the irreducible background. The results of the neutron activation analysis run indicate that the beam density of Ta atoms in the collision region was of the order of $10^7/cm^3$.

2.2.6 The Carbon Source

The e-beam heater described in Section 2.2.5 was used to form a beam of carbon neutral particles. The stability of the beam was not as good as that obtained for tantalum but it was adequate for the measurements. The beam consisted primarily of C, C_2 and C_3 particles with some indication of small quantites of higher polymers being present. Both reactor grade graphite and single crystal graphite substrates were used as target materials in the e-beam device.

2.3 THE APPARATUS FOR OPTICAL STUDIES

The apparatus used for the optical studies was similar in many respects to the crossed beam apparatus used for the charge transfer studies. The primary ions were generated in an ion source, accelerated and the resulting ion beam

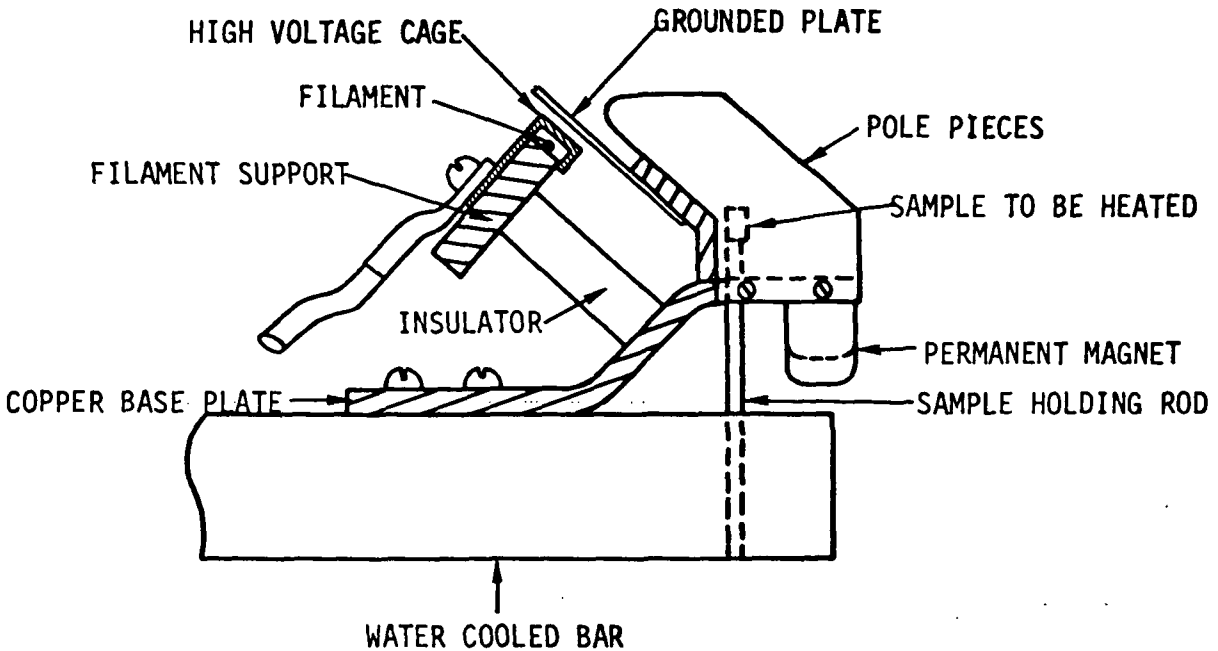

Figure 2. Schematic representation of the electron bombardment heater (e-gun)

analyzed in a magnetic mass spectrometer. The ion source used was of a discharge type to obtain the maximum ion current possible. This source is not suited for low energy cross section measurements because of the large ion energy spread produced. For the work here, we were only interested in the production of radiation and could tolerate the larger energy spread.

The mass analyzed ion beam crossed a quasi beam of metal atoms produced in a manner similar to the way the beam was produced for the charge transfer studies. In order to be able to use phase sensitive detection techniques the ion beam was electrically chopped prior to its interception with the neutral beam. It was necessary here to chop the ion beam since a great deal of dc "noise" was generated by photons from the heated neutral beam furnace.

A schematic of the neutral beam source constructed to produce metal atoms for the optical studies is given in Figure 3. The furnace shown in the diagram is that which was used to form beams of iron atoms.

In addition to heat shields and slits shown in Figure 3, other precautions were taken to minimize the amount of scattered light available which could reach the photon detector. Care was taken to eliminate any surfaces from which photons could be reflected toward the optical system. Further, all surfaces were blacked with carbon soot. The total optical system was mounted in a blackened metal tube such that photons scattered into other parts of the vacuum system could not return to the photon detector.

The optical system constructed for the measurements consisted of two simple convex lens, the first placed such that its focal point lay at the point where the ion beam crossed the quasi neutral beam. The parallel beam of light from this lens was focused by a second lens onto the photocathode of an RCA 31034 phototube. This tube, which has a gallium arsenide photocathode, has very good spectral response for photons in the wavelength range from 250 to 850 nm. Modulation of the ion beam allowed the use of phase sensitive ac amplification techniques which greatly reduced problem associated with stray light.

2.4 ERROR DISCUSSION

Section 2.1.1 discusses the sources of systematic errors, such as determination of the collection efficiency of the secondary ions and the determination of the system gain associated with the charge transfer cross section measurements. The

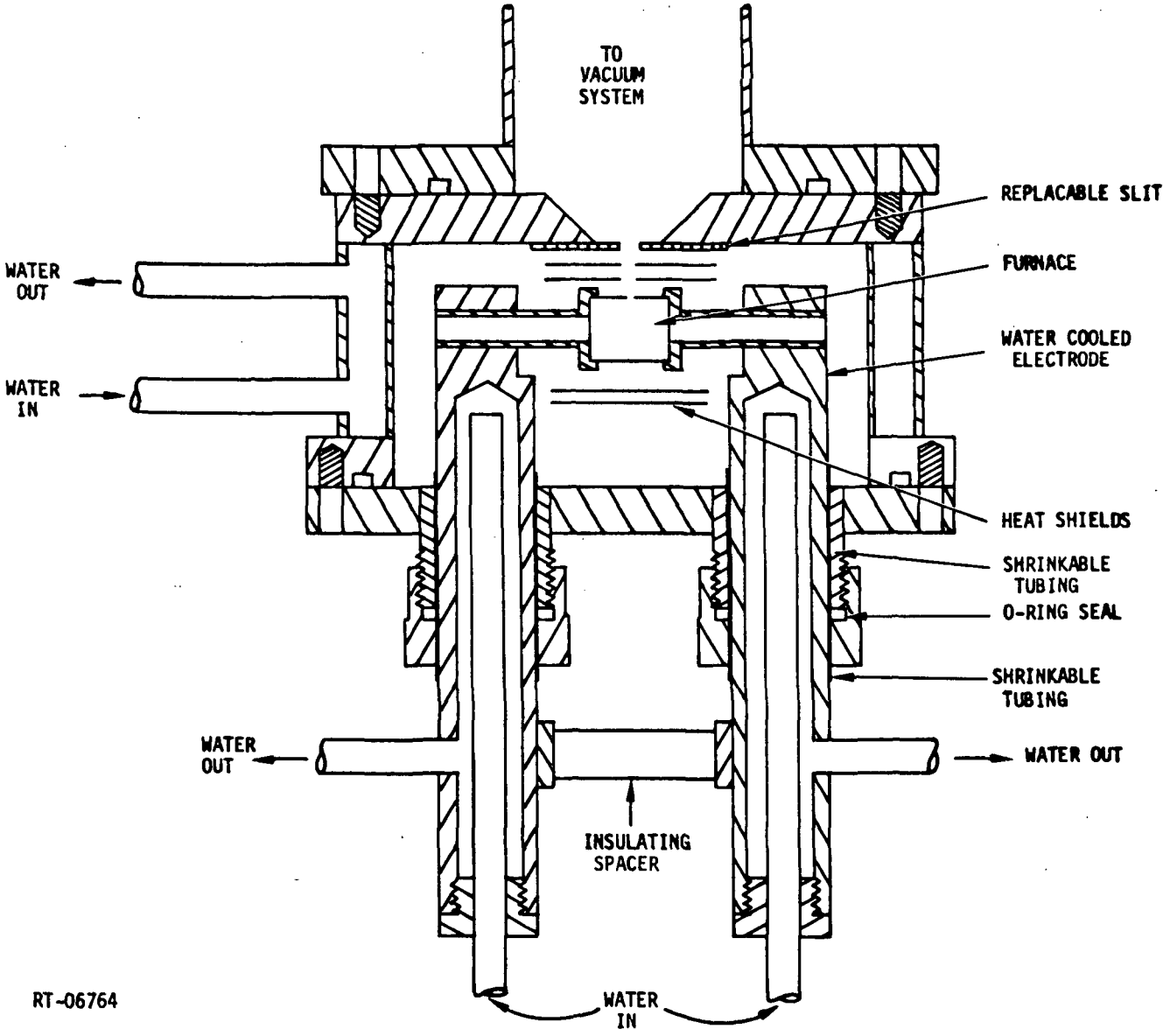

Figure 3. Schematic of metal atom source for optical measurements

possible error introduced in the absolute cross-section determination by these systematic errors is ±15% at high impact energies and increased to ±30% at the lowest energies.

In studies involving metal atoms, an additional possible error is introduced due to the difficulties in determining the neutral beam densities. These added difficulties can increase the possible total error in our measurement to ±50%, depending on the reaction being studied.

3. CHARGE TRANSFER RESULTS AND DISCUSSION

The following sections present the results obtained for the various processes studied. In most cases the results, in both graphical and tabular form, are presented with little or no discussion. The numerous states available in one or both collision partners which may participate in the collision processes has in most cases made an in-depth study of the mechanisms participating beyond the scope of this work. In cases where simple models can be invoked to explain the results obtained, explanations are given.

The data given below are segregated according to the neutral partner involved in the collision. The accuracy of all cross sections given is better than plus or minus a factor of two.

3.1 IRON

Data has been obtained for three primary ions in collisions with neutral iron atoms: Hg^+, Xe^+ and Cs^+. The following paragraphs detail the results obtained.

The results obtained for mercury ions in collision with iron (Reaction 3) are given in Table I and graphically in Figure 4. The slow oscillations in the cross section are believed to be real and can probably be accounted for by new reaction channels opening as the ion energy is increased.

The measured cross sections for Reaction 3 are small when compared with those which have been measured for other charge transfer processes involving metal atoms (cf. References 2 and 10). Such a result may indicate that few channels which are near resonant exist.

Table II gives the results obtained for xenon ions in collision with iron (Reaction 4). These results are presented again in Figure 5. The accuracy of the results is estimated to be better than $\pm$40% over the total energy range studied. The values for the cross sections are similar in magnitude to those measured for Reaction 3, indicating that here again there may not be any channel for which near or exact resonance exists.

Table I. Charge transfer cross sections between Hg^+ and Fe

ION MASS 200.0000
NEUTRAL MASS 56.0000
NEUTRAL BEAM TEMPERATURE 1800.00
NEUTRAL VELOCITY 9.7373+04

ION LAB ENERGY (EV)	COLLISION ENERGY (EV)	CROSS SECTION (CM2)	RATE COEFFICIENT (CM3/SEC)	ION VELOCITY (CM/SEC)	RELATIVE VELOCITY (CM/SEC)
1.00	.43	6.431-16	8.896-11	9.825+04	1.383+05
2.00	.65	7.477-16	1.269-10	1.389+05	1.697+05
3.00	.87	8.314-16	1.630-10	1.702+05	1.961+05
4.00	1.09	7.111-16	1.559-10	1.965+05	2.193+05
5.00	1.31	6.379-16	1.533-10	2.197+05	2.403+05
6.00	1.53	6.491-16	1.685-10	2.407+05	2.596+05
7.00	1.75	7.309-16	2.029-10	2.599+05	2.776+05
8.00	1.96	4.613-16	1.358-10	2.779+05	2.944+05
10.00	2.40	7.282-16	2.371-10	3.107+05	3.256+05
15.00	3.50	5.525-16	2.170-10	3.805+05	3.928+05
20.00	4.59	5.835-16	2.626-10	4.394+05	4.500+05
30.00	6.78	6.427-16	3.515-10	5.381+05	5.469+05
40.00	8.96	6.148-16	3.867-10	6.214+05	6.289+05
50.00	11.15	6.661-16	4.673-10	6.947+05	7.015+05
70.00	15.53	6.510-16	5.389-10	8.220+05	8.277+05
80.00	17.72	5.090-16	4.500-10	8.787+05	8.841+05
90.00	19.90	5.236-16	4.907-10	9.320+05	9.371+05
100.00	22.09	6.566-16	6.483-10	9.825+05	9.873+05
120.00	26.47	8.128-16	8.783-10	1.076+06	1.081+06
150.00	33.03	7.510-16	9.066-10	1.203+06	1.207+06
200.00	43.97	6.318-16	8.800-10	1.389+06	1.393+06
250.00	54.90	5.792-16	9.014-10	1.553+06	1.556+06
300.00	65.84	6.357-16	1.084-09	1.702+06	1.704+06
400.00	87.72	6.000-16	1.180-09	1.965+06	1.967+06
500.00	109.59	7.572-16	1.665-09	2.197+06	2.199+06
600.00	131.47	4.447-16	1.071-09	2.407+06	2.408+06
800.00	175.22	3.975-16	1.105-09	2.779+06	2.781+06
1000.00	218.97	4.350-16	1.352-09	3.107+06	3.108+06
1200.00	262.72	3.909-16	1.331-09	3.403+06	3.405+06
1500.00	328.34	4.457-16	1.696-09	3.805+06	3.806+06
2000.00	437.72	4.919-16	2.162-09	4.394+06	4.395+06
2500.00	547.10	3.762-16	1.848-09	4.912+06	4.913+06
3000.00	656.47	4.552-16	2.450-09	5.381+06	5.382+06
3500.00	765.85	3.847-16	2.237-09	5.812+06	5.813+06
4000.00	875.22	4.651-16	2.890-09	6.214+06	6.214+06
4500.00	984.60	4.197-16	2.766-09	6.591+06	6.591+06
5000.00	1093.98	4.861-16	3.377-09	6.947+06	6.948+06

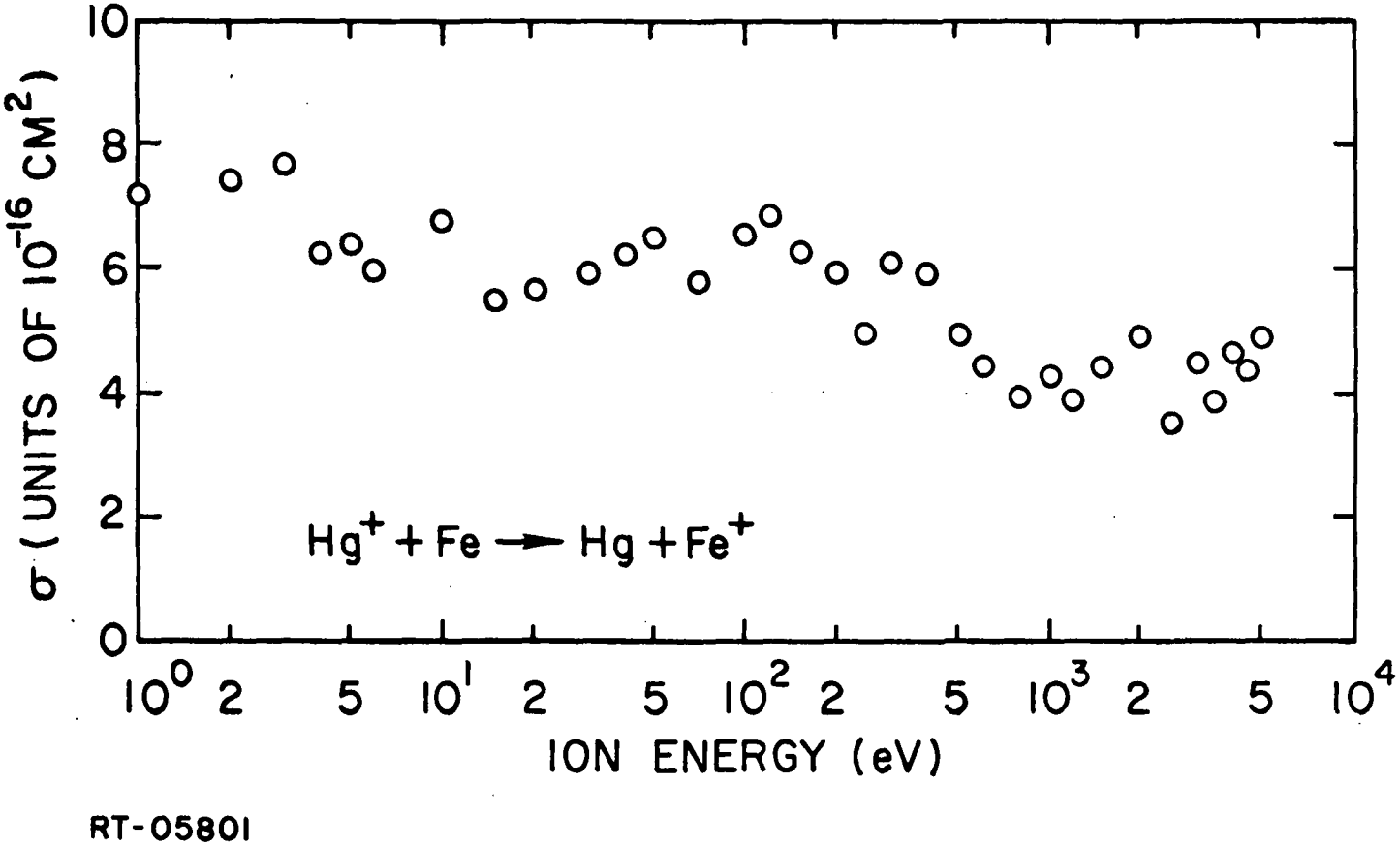

Figure 4. Charge transfer cross sections for mercury ions on iron as a function of the primary ion energy

Table II. Charge transfer cross sections between Xe^+ and Fe

ION MASS 131.0000
NEUTRAL MASS 56.0000
NEUTRAL BEAM TEMPERATURE 1800.00
NEUTRAL VELOCITY 9.7373+04

ION LAB ENERGY (EV)	COLLISION ENERGY (EV)	CROSS SECTION (CM2)	RATE COEFFICIENT (CM3/SEC)	ION VELOCITY (CM/SEC)	RELATIVE VELOCITY (CM/SEC)
1.00	.49	8.329-16	1.296-10	1.214+05	1.556+05
2.00	.79	6.150-16	1.214-10	1.717+05	1.974+05
3.00	1.09	7.344-16	1.702-10	2.103+05	2.317+05
4.00	1.39	7.407-16	1.937-10	2.428+05	2.616+05
5.00	1.69	6.648-16	1.917-10	2.714+05	2.884+05
6.00	1.99	7.227-16	2.261-10	2.973+05	3.129+05
8.00	2.59	7.034-16	2.511-10	3.433+05	3.569+05
10.00	3.19	6.131-16	2.428-10	3.839+05	3.960+05
15.00	4.68	5.860-16	2.814-10	4.702+05	4.801+05
20.00	6.18	6.324-16	3.488-10	5.429+05	5.515+05
25.00	7.68	4.680-16	2.877-10	6.070+05	6.147+05
40.00	12.17	5.201-16	4.025-10	7.678+05	7.739+05
50.00	15.17	4.231-16	3.655-10	8.584+05	8.639+05
60.00	18.16	3.838-16	3.628-10	9.403+05	9.453+05
70.00	21.16	5.208-16	5.313-10	1.016+06	1.020+06
80.00	24.15	3.662-16	3.992-10	1.086+06	1.090+06
100.00	30.14	4.503-16	5.483-10	1.214+06	1.218+06
120.00	36.13	4.129-16	5.505-10	1.330+06	1.333+06
150.00	45.11	3.719-16	5.541-10	1.487+06	1.490+06
180.00	54.10	3.273-16	5.339-10	1.629+06	1.632+06
200.00	60.09	3.710-16	6.380-10	1.717+06	1.720+06
220.00	66.08	3.435-16	6.195-10	1.801+06	1.803+06
221.00	66.38	3.304-16	5.971-10	1.805+06	1.807+06
250.00	75.06	3.455-16	6.640-10	1.919+06	1.922+06
300.00	90.03	3.354-16	7.059-10	2.103+06	2.105+06
350.00	105.01	3.480-16	7.910-10	2.271+06	2.273+06
400.00	119.98	3.400-16	8.261-10	2.428+06	2.430+06
401.00	120.28	3.107-16	7.558-10	2.431+06	2.433+06
450.00	134.95	3.643-16	9.387-10	2.575+06	2.577+06
500.00	149.93	3.215-16	8.732-10	2.714+06	2.716+06
600.00	179.87	2.927-16	8.707-10	2.973+06	2.975+06
700.00	209.82	3.366-16	1.081-09	3.212+06	3.213+06
800.00	239.77	2.778-16	9.542-10	3.433+06	3.435+06
900.00	269.71	3.722-16	1.356-09	3.642+06	3.643+06
1000.00	299.66	2.811-16	1.080-09	3.839+06	3.840+06
1200.00	359.56	2.885-16	1.213-09	4.205+06	4.206+06
1500.00	449.40	3.366-16	1.583-09	4.702+06	4.703+06
1800.00	539.24	3.123-16	1.609-09	5.150+06	5.151+06
2000.00	599.13	3.311-16	1.798-09	5.429+06	5.430+06
2500.00	748.86	4.371-16	2.653-09	6.070+06	6.070+06
3000.00	898.60	3.250-16	2.161-09	6.649+06	6.650+06
3500.00	1048.33	3.497-16	2.511-09	7.182+06	7.182+06
4000.00	1198.07	2.693-16	2.067-09	7.678+06	7.678+06
4500.00	1347.80	3.266-16	2.660-09	8.143+06	8.144+06
5000.00	1497.54	2.889-16	2.480-09	8.584+06	8.584+06

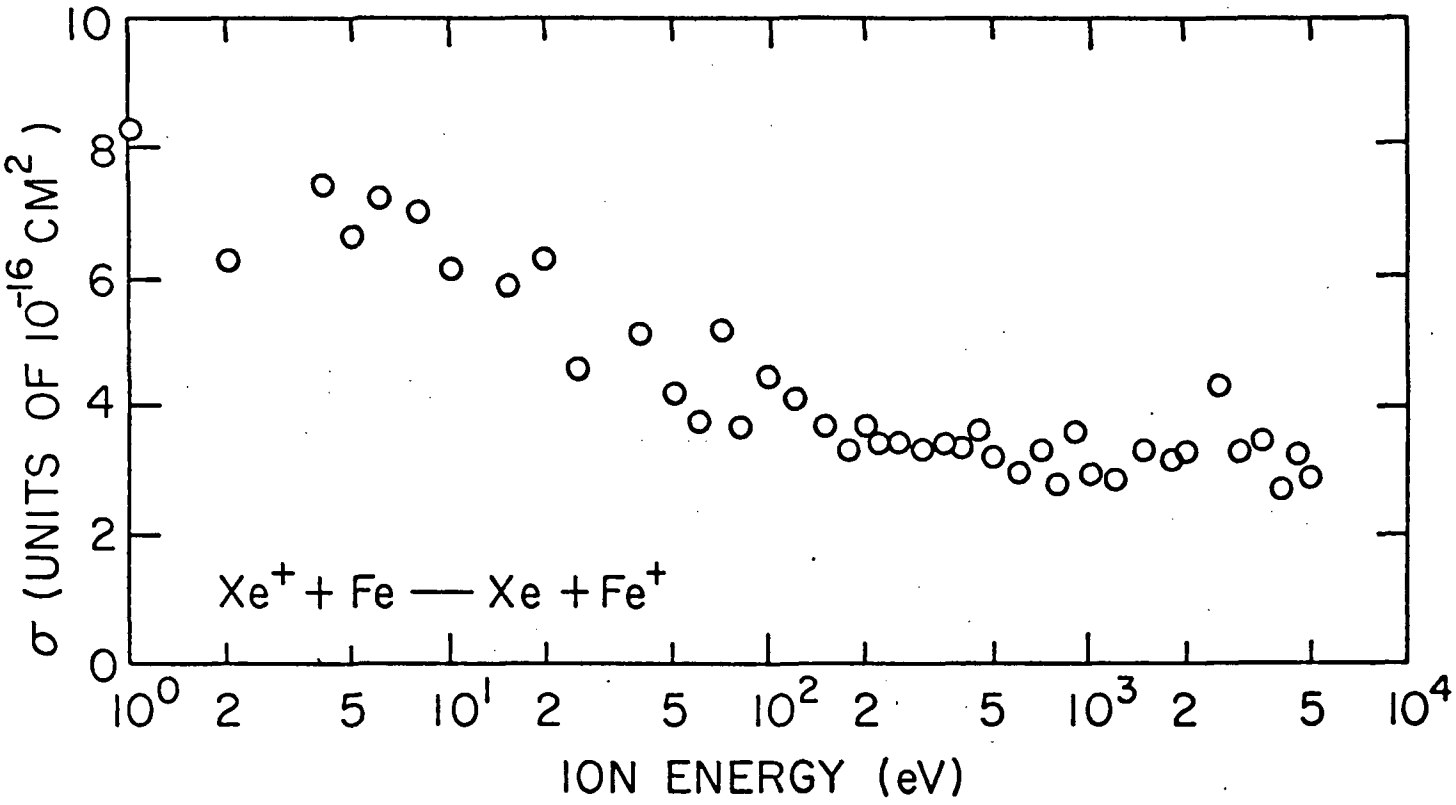

Fig. 5. Charge transfer cross section for xenon ions on iron as a function of the primary ion energy.

In the study of Reaction 5, beams of both Cs^+ and Fe having good stability and adequate density were easily formed. In spite of this, no signals which could be attributed to charge transfer between these species were detected. It was possible, however, to place upper limits on the size of the reaction cross sections. These values are given in Table III.

Table III

Upper limits for the charge transfer cross section between Cs^+ and Fe

Energy (eV)	Upper Limit (cm^2)
5	3.7×10^{-18}
15	1.4×10^{-17}
20	4.0×10^{-18}
60	3.9×10^{-18}
200	7.5×10^{-18}
500	4.1×10^{-18}
1000	2.1×10^{-17}
2000	3.4×10^{-18}
5000	5.1×10^{-18}

Reaction 5 is endothermic and the failure to detect signals for this process is therefore not entirely surprising.

3.2 MOLYBDENUM

Data has been obtained for two primary ions in collision with neutral molybdenum atoms: Hg^+ and Xe^+. The following paragraphs detail the results obtained.

The results obtained for mercury ions in collision with molybdenum (Reaction 1) are given in Table IV and graphically in Figure 6. The main difficulty in the measurement of these cross sections was determining the neutral beam density. In order to obtain the highest possible accuracy in the measurement of the beam density using neutron activation analysis, a reaction with a large charge transfer cross section is desirable. That is, while the neutral beam is being collected to determine the beam density, it is essential to measure a signal due to charge transfer as a calibration point. (The larger the measured signal, the more accurate the calibration.) Past experience has indicated that molecular ions generally have larger cross sections for charge transfer than atomic species

Table IV. Charge transfer cross sections between Hg^+ and Mo

ION MASS 200.0000
NEUTRAL MASS 96.0000
NEUTRAL BEAM TEMPERATURE 2500.00
NEUTRAL VELOCITY 8.7646+04

ION LAB ENERGY (EV)	COLLISION ENERGY (EV)	CROSS SECTION (CM2)	RATE COEFFICIENT (CM3/SEC)	ION VELOCITY (CM/SEC)	RELATIVE VELOCITY (CM/SEC)
1.00	.58	1.482-15	1.951-10	9.825+04	1.317+05
2.00	.91	1.357-15	2.229-10	1.389+05	1.643+05
3.00	1.23	1.338-15	2.562-10	1.702+05	1.914+05
4.00	1.56	1.284-15	2.763-10	1.965+05	2.152+05
5.00	1.88	1.380-15	3.265-10	2.197+05	2.365+05
6.00	2.20	1.357-15	3.475-10	2.407+05	2.561+05
7.00	2.53	1.149-15	3.151-10	2.599+05	2.743+05
8.00	2.85	1.436-15	4.184-10	2.779+05	2.914+05
10.00	3.50	1.300-15	4.196-10	3.107+05	3.228+05
12.00	4.15	1.300-15	4.569-10	3.403+05	3.514+05
15.00	5.12	1.300-15	5.076-10	3.805+05	3.905+05
18.00	6.10	1.475-15	6.281-10	4.168+05	4.259+05
20.00	6.74	1.308-15	5.861-10	4.394+05	4.480+05
25.00	8.37	1.044-15	5.208-10	4.912+05	4.990+05
40.00	13.23	1.093-15	6.857-10	6.214+05	6.275+05
100.00	32.69	8.667-16	8.548-10	9.825+05	9.864+05
200.00	65.12	7.647-16	1.065-09	1.389+06	1.392+06
300.00	97.56	9.644-16	1.643-09	1.702+06	1.704+06
400.00	129.99	1.021-15	2.009-09	1.965+06	1.967+06
500.00	162.42	9.202-16	2.023-09	2.197+06	2.199+06
600.00	194.85	7.101-16	1.710-09	2.407+06	2.408+06
700.00	227.29	7.831-16	2.037-09	2.599+06	2.601+06
800.00	259.72	8.328-16	2.315-09	2.779+06	2.780+06
900.00	292.15	6.852-16	2.020-09	2.947+06	2.949+06
1000.00	324.59	7.203-16	2.239-09	3.107+06	3.108+06
2000.00	648.91	6.933-16	3.047-09	4.394+06	4.395+06
2500.00	811.08	6.985-16	3.432-09	4.912+06	4.913+06
4000.00	1297.57	8.320-16	5.170-09	6.214+06	6.214+06
5000.00	1621.90	8.320-16	5.780-09	6.947+06	6.948+06

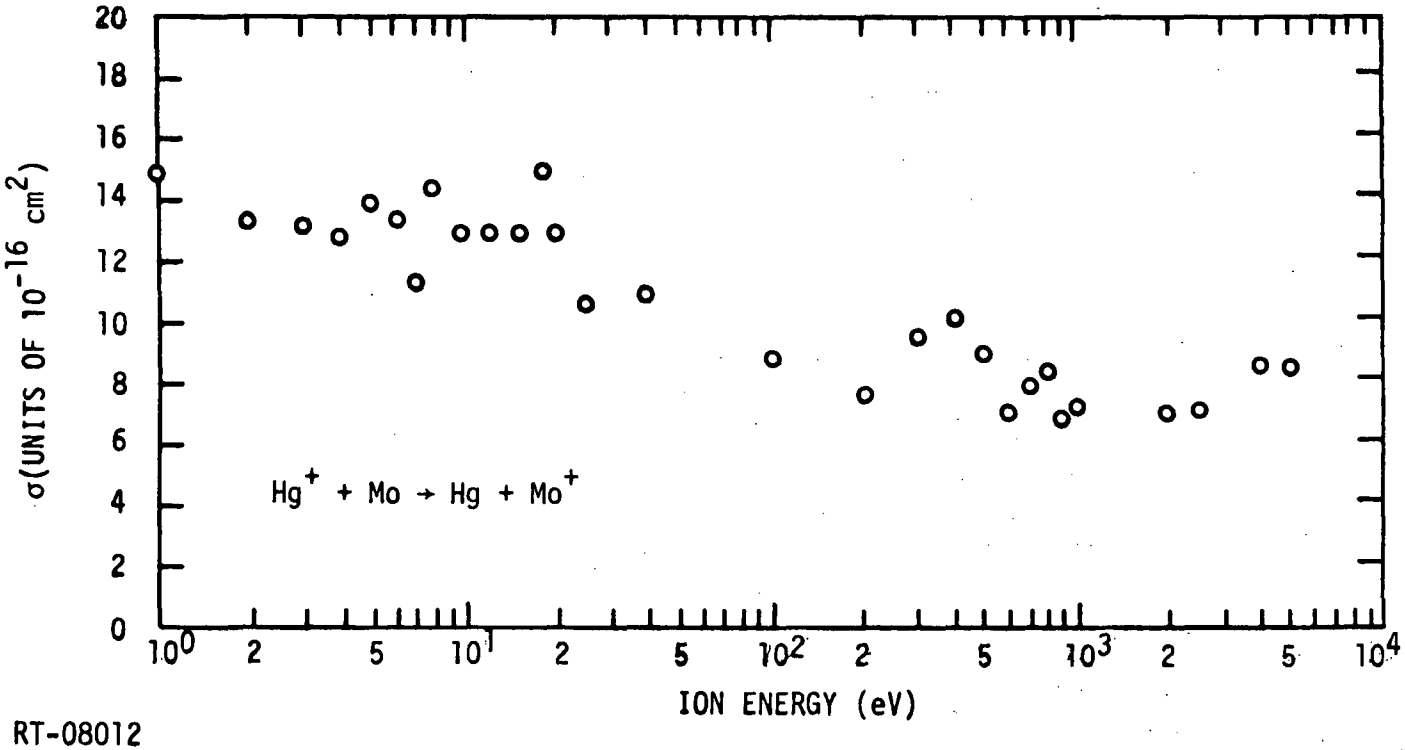

Figure 6. Cross section for charge transfer from Hg^+ to Mo as a function of the primary ion energy

(see References 2, 10 and 11). For molybdenum, it is found that the signal for the N_2^+ reaction with Mo to give Mo^+ is about ten times those of the atomic species of interest. The reaction of this molecular ion was therefore chosen for calibration on the neutral beam. Figure 7 gives the cross section as a function of ion energy for N_2^+ charge transfer with Mo in the range from 1 to 1000 eV. Data for this reaction was obtained using both types of Mo atom sources (see Section 2.2.2). Using this reaction, together with the neutron activation analysis, it was possible to determine the Mo beam density to within $\pm$30%.

Examination of the data in Figure 6 shows considerable scatter in the data for Reaction 1. The scatter reflects the difficulties encountered in these measurements. The difficulties can be enumerated as

1. Low density of the Mo neutral beam.
2. Relatively short lifetime of the Mo furnaces.
3. Experimental noise associated with the use of a primary ion heavier than the neutral target.

Figure 8 and Table V give the data obtained for xenon ions in collision with molybdenum (Reaction 2). In general, the scattering in the Xe^+ data is less than that found for the Hg^+ results given above. This improvement comes about because of the larger primary Xe^+ ion beams which can be generated in our ion source. We have no reason to discount the apparent increase in the cross section at 8 eV ion energy.

3.3 ALUMINUM

Data has been obtained for three primary ions in collision with neutral aluminum atoms: Hg^+, Xe^+ and Cs^+. The following paragraphs detail the results obtained.

For aluminum, it was not possible to use neutron activation analysis to obtain the neutral beam density. We therefore have relied on Knudsen cell calculations to establish our cross sections.

The use of the Knudsen cell calculations is justified for several reasons. Past experience in the use of high temperature has shown that if the vapor pressure in the cell is correct at a given temperature, and if any change in temperature of the cell produces the correct change in pressure (correct temperature dependence), then the density in a beam produced from the cell can be calculated from the known

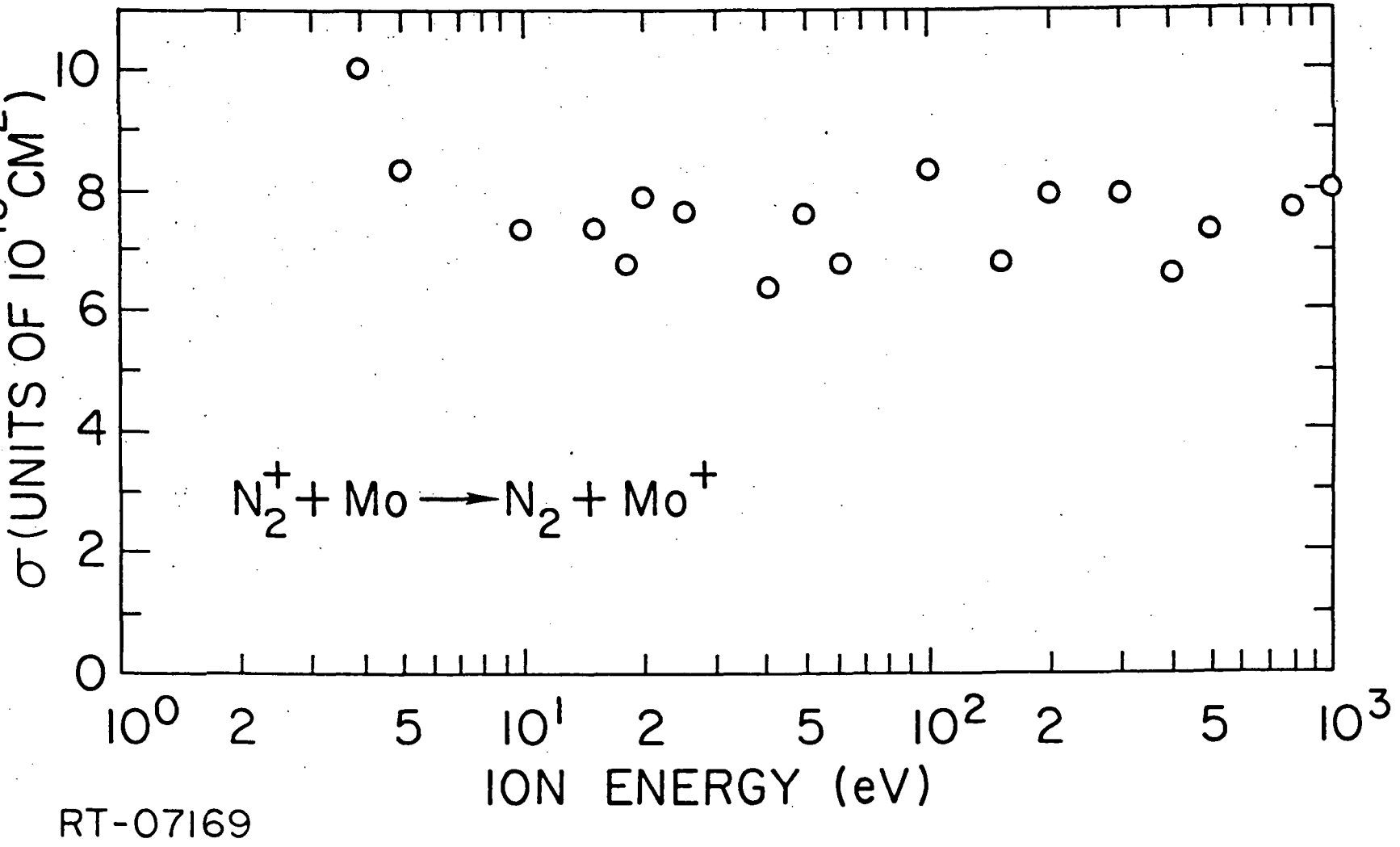

Figure 7. Cross section for charge transfer from N_2^+ to Mo as a function of the ion energy

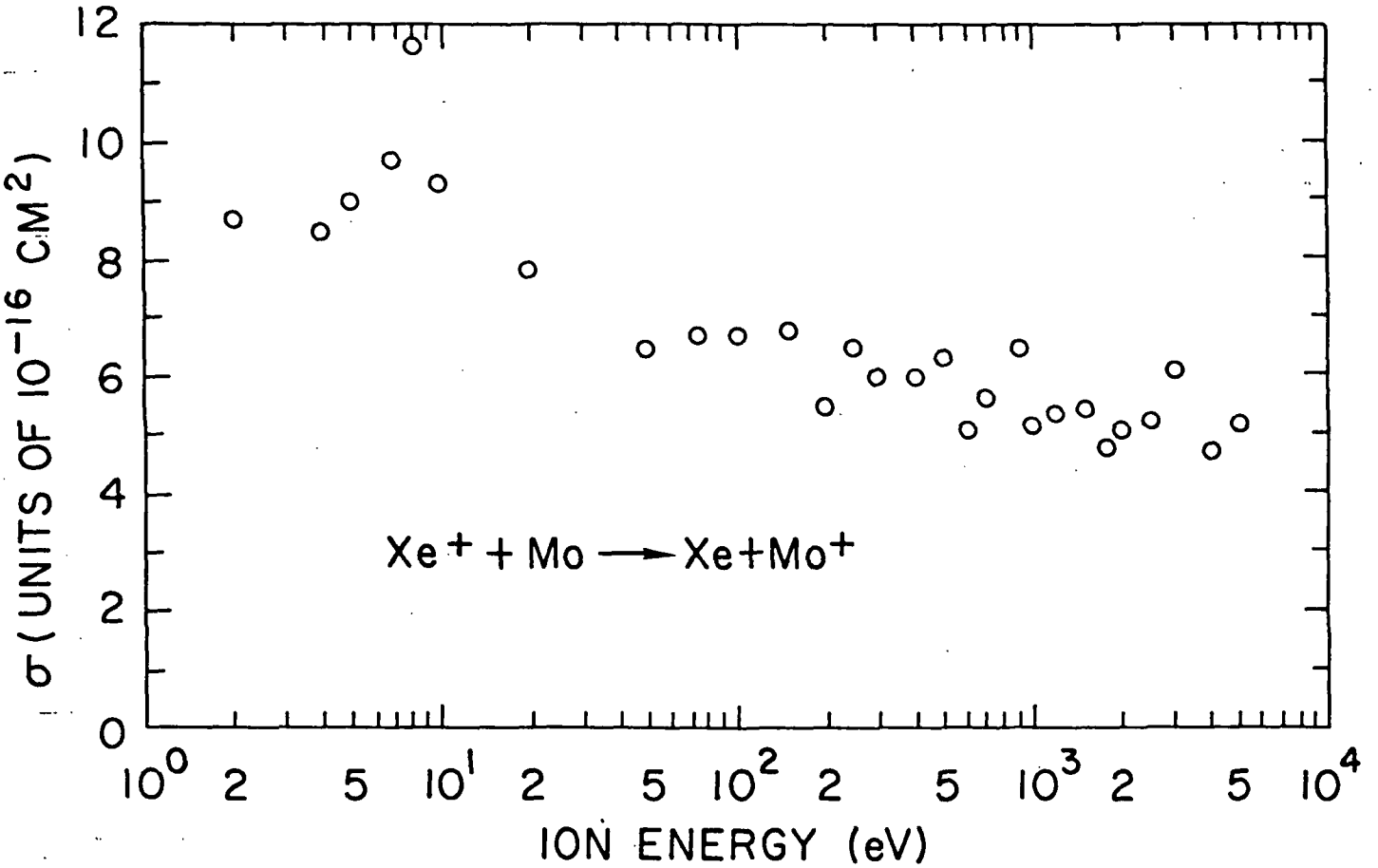

Figure 8. Cross section for charge transfer from Xe^+ to Mo^+ as a function of the primary energy

Table V. Charge transfer cross sections between Xe^+ and Mo

ION MASS 131.0000
NEUTRAL MASS 96.0000
NEUTRAL BEAM TEMPERATURE 2500.00
NEUTRAL VELOCITY 8.7646+04

ION LAB ENERGY (EV)	COLLISION ENERGY (EV)	CROSS SECTION (CM2)	RATE COEFFICIENT (CM3/SEC)	ION VELOCITY (CM/SEC)	RELATIVE VELOCITY (CM/SEC)
2.00	1.07	8.675-16	1.672-10	1.717+05	1.928+05
4.00	1.91	8.489-16	2.191-10	2.428+05	2.581+05
5.00	2.34	9.001-16	2.568-10	2.714+05	2.852+05
7.00	3.18	9.676-16	3.221-10	3.212+05	3.329+05
8.00	3.60	1.197-15	4.243-10	3.433+05	3.544+05
10.00	4.45	9.377-16	3.692-10	3.839+05	3.938+05
20.00	8.68	7.843-16	4.313-10	5.429+05	5.499+05
50.00	21.37	6.530-16	5.634-10	8.584+05	8.628+05
75.00	31.94	6.743-16	7.114-10	1.051+06	1.055+06
100.00	42.51	6.726-16	8.186-10	1.214+06	1.217+06
150.00	63.66	6.805-16	1.013-09	1.487+06	1.489+06
200.00	84.80	5.520-16	9.489-10	1.717+06	1.719+06
250.00	105.95	6.564-16	1.261-09	1.919+06	1.921+06
300.00	127.09	6.016-16	1.266-09	2.103+06	2.104+06
400.00	169.39	6.000-16	1.458-09	2.428+06	2.429+06
500.00	211.68	6.362-16	1.728-09	2.714+06	2.716+06
600.00	253.97	5.111-16	1.520-09	2.973+06	2.975+06
700.00	296.26	5.614-16	1.804-09	3.212+06	3.213+06
900.00	380.84	6.561-16	2.390-09	3.642+06	3.643+06
1000.00	423.13	5.167-16	1.984-09	3.839+06	3.840+06
1200.00	507.72	5.373-16	2.260-09	4.205+06	4.206+06
1500.00	634.59	5.424-16	2.551-09	4.702+06	4.702+06
1800.00	761.46	4.805-16	2.475-09	5.150+06	5.151+06
2000.00	846.05	5.079-16	2.758-09	5.429+06	5.430+06
2500.00	1057.50	5.227-16	3.173-09	6.070+06	6.070+06
3000.00	1268.96	6.103-16	4.059-09	6.649+06	6.650+06
4000.00	1691.87	4.636-16	3.559-09	7.678+06	7.678+06
5000.00	2114.78	5.193-16	4.458-09	8.584+06	8.584+06

pressure. That is, in cases where the cell appeared to operate as a true Knudsen cell, the beam densities obtained by calculation, and those obtained from activation analysis were in good agreement. For aluminum the cell operated as one would expect.

Table VI gives numerical data for the reaction of mercury ions with aluminum (Reaction 6). Graphical data is given in Figure 9. The values given are considered to be accurate within a factor of 2.

The results for xenon ions in collision with aluminum atoms (Reaction 7) are given in Table VII and Figure 10.

The charge transfer process between cesium ions and aluminum (Reaction 8) is endothermic and might be expected to exhibit a threshold for reaction. The results obtained, however, showed that in the energy range from 1 to 5000 eV, the cross section for reaction is below the detection limit of our apparatus. Upper limits have, however, been obtained for this process. These values are given in Table VIII.

Table VIII

Upper limits for the charge transfer cross section between Cs^+ and Al

Ion Energy (eV)	Upper Limit (cm^2)
10	5×10^{-18}
20	2×10^{-18}
30	3×10^{-18}
50	3×10^{-18}
100	2×10^{-18}
200	6×10^{-19}
300	5×10^{-18}
500	3×10^{-18}
700	5×10^{-19}
1000	3×10^{-19}
2000	6×10^{-18}
3000	9×10^{-18}
5000	1×10^{-18}

Table VI. Charge transfer cross sections between Hg^+ and Al

ION MASS 200.0000
NEUTRAL MASS 27.0000
NEUTRAL BEAM TEMPERATURE 1590.00
NEUTRAL VELOCITY 1.3180+05

ION LAB ENERGY (EV)	COLLISION ENERGY (EV)	CROSS SECTION (CM2)	RATE COEFFICIENT (CM3/SEC)	ION VELOCITY (CM/SEC)	RELATIVE VELOCITY (CM/SEC)
1.00	.33	3.947-16	6.489-11	9.825+04	1.644+05
2.00	.45	4.553-16	8.719-11	1.389+05	1.915+05
3.00	.57	4.410-16	9.492-11	1.702+05	2.152+05
4.00	.69	4.990-16	1.181-10	1.965+05	2.366+05
5.00	.81	5.267-16	1.349-10	2.197+05	2.562+05
6.00	.93	5.192-16	1.425-10	2.407+05	2.744+05
7.00	1.05	4.835-16	1.409-10	2.599+05	2.914+05
8.00	1.17	4.888-16	1.503-10	2.779+05	3.076+05
9.00	1.28	4.670-16	1.508-10	2.947+05	3.229+05
10.00	1.40	5.604-16	1.891-10	3.107+05	3.375+05
12.00	1.64	5.399-16	1.971-10	3.403+05	3.650+05
15.00	2.00	5.306-16	2.137-10	3.805+05	4.027+05
18.00	2.36	5.006-16	2.188-10	4.168+05	4.372+05
20.00	2.59	4.944-16	2.268-10	4.394+05	4.587+05
25.00	3.19	5.054-16	2.570-10	4.912+05	5.086+05
30.00	3.78	4.824-16	2.672-10	5.381+05	5.540+05
40.00	4.97	4.341-16	2.758-10	6.214+05	6.352+05
50.00	6.16	4.262-16	3.014-10	6.947+05	7.071+05
60.00	7.35	3.759-16	2.903-10	7.610+05	7.723+05
70.00	8.54	3.627-16	3.020-10	8.220+05	8.325+05
80.00	9.73	3.763-16	3.344-10	8.787+05	8.886+05
100.00	12.11	3.644-16	3.612-10	9.825+05	9.913+05
120.00	14.49	3.401-16	3.688-10	1.076+06	1.084+06
150.00	18.06	4.090-16	4.951-10	1.203+06	1.210+06
180.00	21.62	3.840-16	5.087-10	1.318+06	1.325+06
200.00	24.00	3.432-16	4.789-10	1.389+06	1.396+06
220.00	26.38	3.609-16	5.281-10	1.457+06	1.463+06
250.00	29.95	3.869-16	6.032-10	1.553+06	1.559+06
280.00	33.52	4.252-16	7.012-10	1.644+06	1.649+06
300.00	35.90	3.656-16	6.239-10	1.702+06	1.707+06
350.00	41.84	4.088-16	7.532-10	1.838+06	1.843+06
400.00	47.79	3.800-16	7.483-10	1.965+06	1.969+06
500.00	59.69	4.603-16	1.013-09	2.197+06	2.201+06
600.00	71.58	5.196-16	1.252-09	2.407+06	2.410+06
700.00	83.47	5.258-16	1.368-09	2.599+06	2.603+06
800.00	95.37	4.685-16	1.303-09	2.779+06	2.782+06
1000.00	119.16	4.754-16	1.478-09	3.107+06	3.110+06
1200.00	142.95	4.370-16	1.489-09	3.403+06	3.406+06
1500.00	178.63	4.869-16	1.854-09	3.805+06	3.807+06
1800.00	214.31	4.606-16	1.921-09	4.168+06	4.170+06
2000.00	238.10	7.938-16	3.489-09	4.394+06	4.396+06
2500.00	297.57	5.650-16	2.776-09	4.912+06	4.914+06
3000.00	357.05	6.132-16	3.300-09	5.381+06	5.383+06
3500.00	416.52	7.139-16	4.151-09	5.812+06	5.814+06
4000.00	475.99	6.721-16	4.177-09	6.214+06	6.215+06
4500.00	535.46	5.952-16	3.924-09	6.591+06	6.592+06
5000.00	594.93	5.702-16	3.962-09	6.947+06	6.948+06

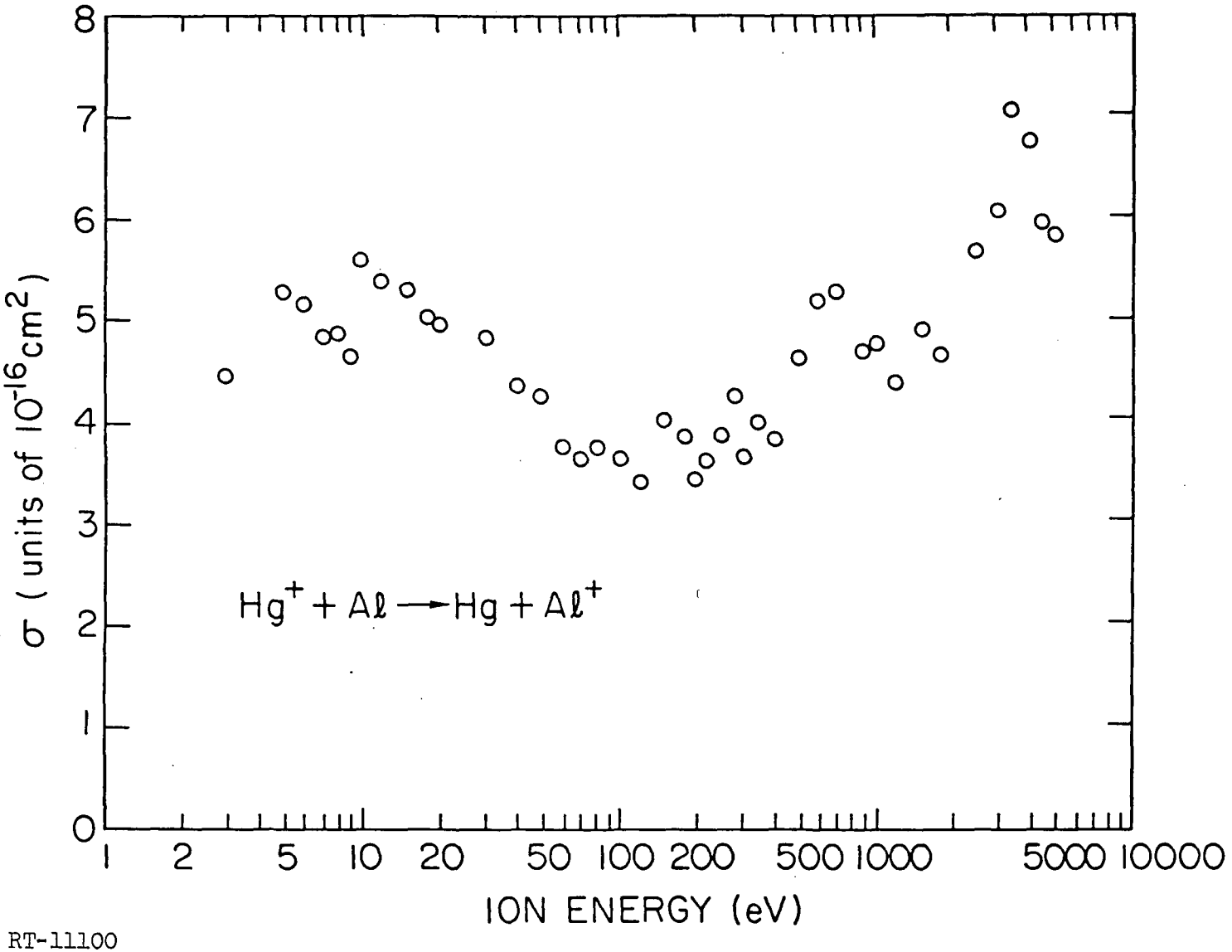

RT-11100

Figure 9. Cross section for charge transfer from Hg^+ to Al as a function of the primary ion energy

Table VII. Charge transfer cross sections between Xe^+ and Al

ION MASS 133.0000
NEUTRAL MASS 27.0000
NEUTRAL BEAM TEMPERATURE 1590.00
NEUTRAL VELOCITY 1.3180+05

ION LAB ENERGY (EV)	COLLISION ENERGY (EV)	CROSS SECTION (CM2)	RATE COEFFICIENT (CM3/SEC)	ION VELOCITY (CM/SEC)	RELATIVE VELOCITY (CM/SEC)
1.00	.37	1.691-15	3.020-10	1.205+05	1.786+05
2.00	.54	1.537-15	3.311-10	1.704+05	2.154+05
3.00	.71	1.401-15	3.457-10	2.087+05	2.468+05
4.00	.88	1.300-15	3.571-10	2.410+05	2.746+05
5.00	1.05	1.234-15	3.700-10	2.694+05	2.999+05
6.00	1.21	1.196-15	3.867-10	2.951+05	3.232+05
7.00	1.38	1.128-15	3.889-10	3.188+05	3.449+05
8.00	1.55	1.146-15	4.186-10	3.408+05	3.654+05
9.00	1.72	1.113-15	4.281-10	3.614+05	3.847+05
10.00	1.89	9.740-16	3.926-10	3.810+05	4.031+05
12.00	2.23	9.909-16	4.337-10	4.173+05	4.377+05
15.00	2.73	9.758-16	4.731-10	4.666+05	4.849+05
18.00	3.24	9.095-16	4.801-10	5.111+05	5.279+05
20.00	3.58	7.725-16	4.285-10	5.388+05	5.547+05
25.00	4.42	7.395-16	4.560-10	6.024+05	6.166+05
30.00	5.26	7.795-16	5.246-10	6.599+05	6.729+05
40.00	6.95	7.228-16	5.589-10	7.620+05	7.733+05
50.00	8.64	5.840-16	5.035-10	8.519+05	8.620+05
60.00	10.33	6.297-16	5.934-10	9.332+05	9.425+05
70.00	12.01	5.638-16	5.731-10	1.008+06	1.017+06
80.00	13.70	5.197-16	5.641-10	1.078+06	1.086+06
100.00	17.08	4.674-16	5.664-10	1.205+06	1.212+06
120.00	20.45	4.720-16	6.261-10	1.320+06	1.326+06
150.00	25.51	4.196-16	6.216-10	1.476+06	1.481+06
180.00	30.58	3.947-16	6.400-10	1.616+06	1.622+06
200.00	33.95	4.105-16	7.015-10	1.704+06	1.709+06
220.00	37.33	4.457-16	7.986-10	1.787+06	1.792+06
250.00	42.39	4.425-16	8.450-10	1.905+06	1.909+06
300.00	50.83	4.632-16	9.684-10	2.087+06	2.091+06
350.00	59.27	3.844-16	8.679-10	2.254+06	2.258+06
400.00	67.70	4.000-16	9.653-10	2.410+06	2.413+06
450.00	76.14	3.954-16	1.012-09	2.556+06	2.559+06
500.00	84.58	3.683-16	9.933-10	2.694+06	2.697+06
600.00	101.45	2.070-16	6.114-10	2.951+06	2.954+06
700.00	118.33	1.939-16	6.187-10	3.188+06	3.190+06
800.00	135.20	1.243-16	4.239-10	3.408+06	3.410+06
900.00	152.08	1.748-16	6.321-10	3.614+06	3.617+06
1000.00	168.95	1.524-16	5.810-10	3.810+06	3.812+06
1200.00	202.70	2.469-16	1.031-09	4.173+06	4.176+06
1500.00	253.33	2.192-16	1.023-09	4.666+06	4.668+06
1800.00	303.96	3.385-16	1.731-09	5.111+06	5.113+06
2000.00	337.71	2.783-16	1.500-09	5.388+06	5.389+06
2500.00	422.08	4.577-16	2.758-09	6.024+06	6.025+06
3000.00	506.46	4.264-16	2.814-09	6.599+06	6.600+06
3500.00	590.83	5.628-16	4.012-09	7.127+06	7.129+06
4000.00	675.21	5.045-16	3.845-09	7.620+06	7.621+06
4500.00	759.59	6.103-16	4.933-09	8.082+06	8.083+06
5000.00	843.96	5.040-16	4.294-09	8.519+06	8.520+06

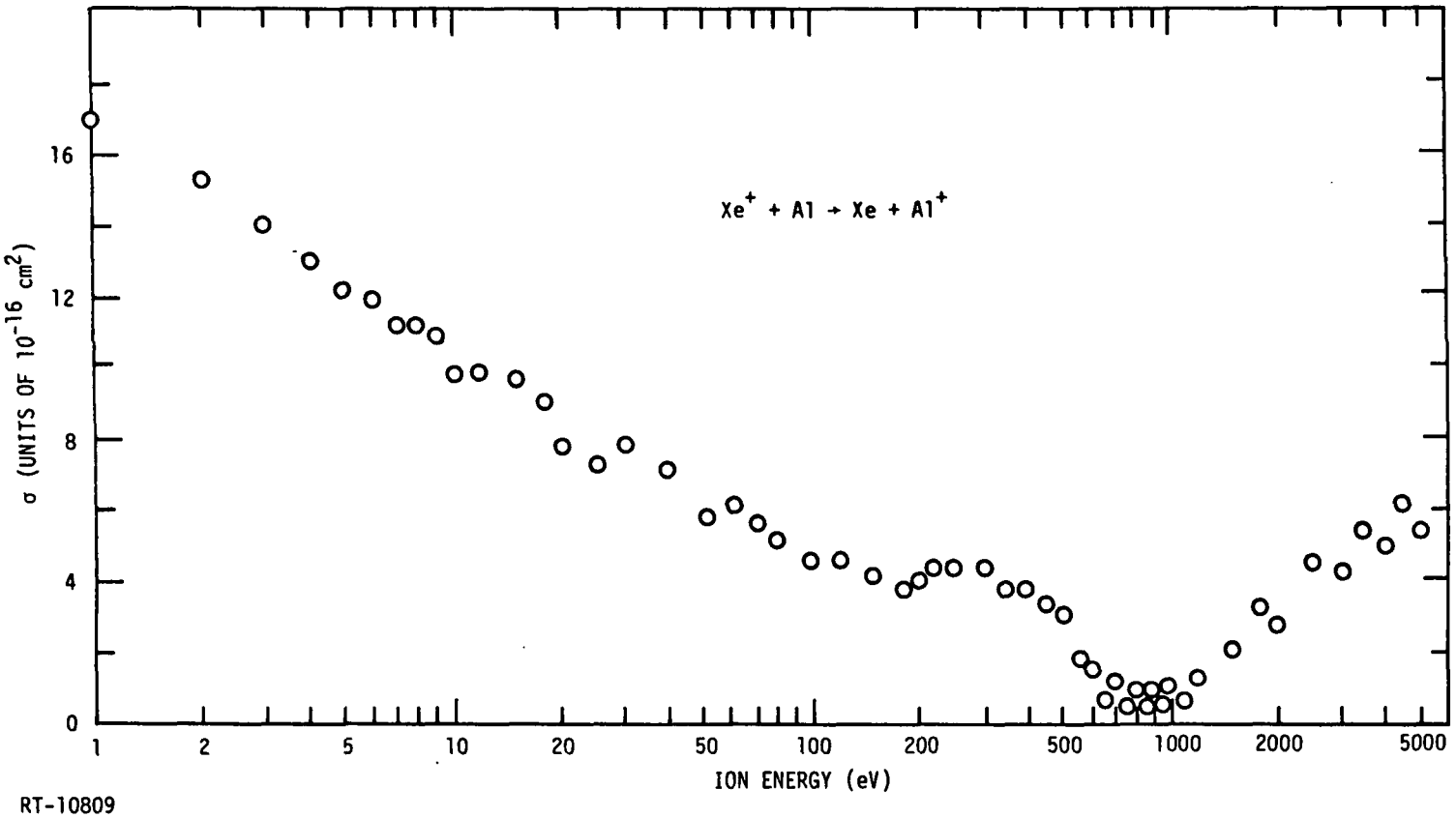

Figure 10. Cross section for charge transfer from Xe^+ to Al as a function of the primary ion energy

3.4 TITANIUM

Data has been obtained for two primary ions in collision with neutral titanium atoms: Hg^+ and Xe^+. The following paragraphs outline the results obtained.

As discussed in Section 2.2.4, some problems were initially encountered in the operation of the titanium metal atom source. Once these problems were overcome, the measurement of the required cross sections were completed with a minimum of trouble.

Table IX gives numerical values for the charge transfer cross section between mercury ions and titanium (Reaction 9). Figure 11 presents the data in graphical form.

The cross sections measured for the charge transfer between xenon ions and titanium (Reaction 10) are presented in Table X and graphically in Figure 12.

3.5 TANTALUM

Data has been obtained for mercury ions in collision with tantalum atoms. Once a suitable e-beam heater had been developed to produce usable beams of this material the measurements were carried out without serious problems. Tests were performed to identify any dimers or phigher polymers in the beam. These tests indicated that no species other than monomers were present in any concentration which would interfere with the measurements.

Table XI presents the numerical values we obtained for the charge transfer cross section between mercury ions and tantalum atoms (Reaction 11). Figure 13 displays the data obtained.

As discussed in Section 2.2.5, the e-beam heater source produced an irreducible signal in our measurements of charge transfer processes. This signal could be subtracted out in most cases but difficulties were encountered at low primary ion energies. For Ta, it was therefore impossible to get usable measurements below 10 eV ion energy. It is possible from our measurement, however, to say that the cross section for reaction does not increase significantly in the ion energy region between 1 and 10 eV.

Table IX. Charge transfer cross sections between Hg^+ and Ti

ION MASS 200.0000
NEUTRAL MASS 48.0000
NEUTRAL BEAM TEMPERATURE 1925.00
NEUTRAL VELOCITY 1.0877+05

ION LAB ENERGY (EV)	COLLISION ENERGY (EV)	CROSS SECTION (CM2)	RATE COEFFICIENT (CM3/SEC)	ION VELOCITY (CM/SEC)	RELATIVE VELOCITY (CM/SEC)
2.10	.64	2.405-15	4.309-10	1.424+05	1.792+05
2.50	.72	2.546-15	4.828-10	1.553+05	1.896+05
3.20	.86	2.057-15	4.251-10	1.757+05	2.067+05
3.80	.97	2.106-15	4.638-10	1.915+05	2.202+05
4.00	1.01	2.115-15	4.750-10	1.965+05	2.246+05
4.30	1.07	1.910-15	4.411-10	2.037+05	2.309+05
5.00	1.20	2.063-15	5.057-10	2.197+05	2.451+05
6.00	1.40	2.053-15	5.422-10	2.407+05	2.641+05
7.00	1.59	2.096-15	5.906-10	2.599+05	2.818+05
8.00	1.79	2.048-15	6.111-10	2.779+05	2.984+05
10.00	2.17	1.850-15	6.090-10	3.107+05	3.292+05
12.00	2.56	2.106-15	7.525-10	3.403+05	3.573+05
15.00	3.14	2.067-15	8.180-10	3.805+05	3.957+05
18.00	3.72	1.959-15	8.439-10	4.168+05	4.308+05
20.00	4.11	1.851-15	8.378-10	4.394+05	4.526+05
25.00	5.08	2.162-15	1.088-09	4.912+05	5.031+05
30.00	6.04	1.851-15	1.016-09	5.381+05	5.490+05
40.00	7.98	2.198-15	1.387-09	6.214+05	6.308+05
50.00	9.91	2.008-15	1.412-09	6.947+05	7.032+05
60.00	11.85	2.092-15	1.608-09	7.610+05	7.687+05
70.00	13.79	2.184-15	1.811-09	8.220+05	8.291+05
80.00	15.72	2.295-15	2.032-09	8.787+05	8.854+05
100.00	19.59	2.405-15	2.377-09	9.825+05	9.885+05
120.00	23.46	2.154-15	2.330-09	1.076+06	1.082+06
125.00	24.43	2.071-15	2.286-09	1.098+06	1.104+06
150.00	29.27	2.144-15	2.590-09	1.203+06	1.208+06
180.00	35.08	2.035-15	2.691-09	1.318+06	1.323+06
200.00	38.95	2.181-15	3.040-09	1.389+06	1.394+06
220.00	42.82	2.106-15	3.077-09	1.457+06	1.461+06
250.00	48.62	2.558-15	3.983-09	1.553+06	1.557+06
280.00	54.43	2.377-15	3.916-09	1.644+06	1.648+06
300.00	58.30	2.621-15	4.469-09	1.702+06	1.705+06
325.00	63.14	2.721-15	4.828-09	1.771+06	1.774+06
350.00	67.98	2.602-15	4.791-09	1.838+06	1.841+06
380.00	73.79	2.830-15	5.429-09	1.915+06	1.918+06
400.00	77.66	2.938-15	5.782-09	1.965+06	1.968+06
450.00	87.34	2.938-15	6.131-09	2.084+06	2.087+06
500.00	97.01	3.258-15	7.166-09	2.197+06	2.200+06
550.00	106.69	3.310-15	7.635-09	2.304+06	2.307+06
600.00	116.37	3.330-15	8.022-09	2.407+06	2.409+06
700.00	135.72	3.428-15	8.918-09	2.599+06	2.602+06
800.00	155.08	3.601-15	1.001-08	2.779+06	2.781+06
900.00	174.43	3.477-15	1.025-08	2.947+06	2.949+06
1000.00	193.79	3.624-15	1.127-08	3.107+06	3.109+06
1200.00	232.50	3.379-15	1.151-08	3.403+06	3.405+06
1500.00	290.56	3.453-15	1.314-08	3.805+06	3.807+06
1800.00	348.63	3.820-15	1.593-08	4.168+06	4.170+06
2000.00	387.34	4.065-15	1.787-08	4.394+06	4.395+06
2500.00	484.11	3.869-15	1.901-08	4.912+06	4.913+06
3000.00	580.89	4.065-15	2.188-08	5.381+06	5.382+06
3500.00	677.66	4.408-15	2.563-08	5.812+06	5.813+06
4000.00	774.44	4.702-15	2.922-08	6.214+06	6.215+06
4500.00	871.22	4.496-15	2.963-08	6.591+06	6.591+06
5000.00	967.99	4.757-15	3.305-08	6.947+06	6.948+06

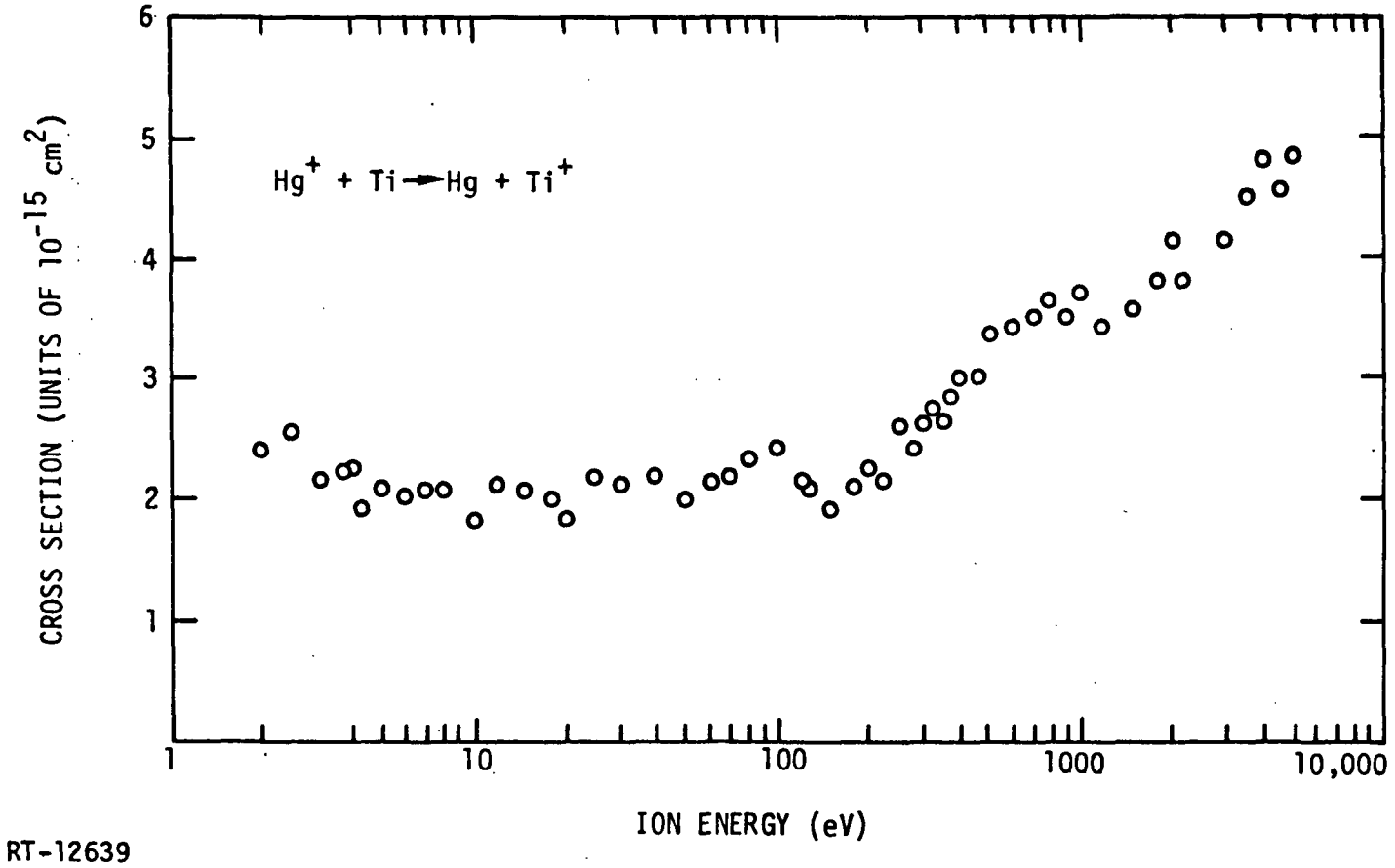

Figure 11. Cross section for charge transfer from Hg^+ to Ti as a function of primary ion energy

Table X. Charge transfer cross sections between Xe^+ and Ti

ION MASS 131.0000
NEUTRAL MASS 48.0000
NEUTRAL BEAM TEMPERATURE 1925.00
NEUTRAL VELOCITY 1.0877+05

ION LAB ENERGY (EV)	COLLISION ENERGY (EV)	CROSS SECTION (CM2)	RATE COEFFICIENT (CM3/SEC)	ION VELOCITY (CM/SEC)	RELATIVE VELOCITY (CM/SEC)
3.70	1.21	8.411-16	2.167-10	2.335+05	2.576+05
4.70	1.48	8.333-16	2.373-10	2.632+05	2.848+05
5.00	1.56	8.333-16	2.437-10	2.714+05	2.924+05
6.00	1.82	7.919-16	2.507-10	2.973+05	3.166+05
7.00	2.09	8.228-16	2.790-10	3.212+05	3.391+05
8.00	2.36	8.400-16	3.025-10	3.433+05	3.602+05
9.00	2.63	8.322-16	3.163-10	3.642+05	3.801+05
10.00	2.90	8.322-16	3.320-10	3.839+05	3.990+05
12.00	3.43	8.213-16	3.567-10	4.205+05	4.344+05
15.00	4.24	7.867-16	3.796-10	4.702+05	4.826+05
18.00	5.04	8.177-16	4.304-10	5.150+05	5.264+05
20.00	5.58	7.963-16	4.409-10	5.429+05	5.537+05
22.00	6.11	7.963-16	4.616-10	5.694+05	5.797+05
25.00	6.92	7.786-16	4.801-10	6.070+05	6.166+05
30.00	8.26	7.867-16	5.300-10	6.649+05	6.737+05
40.00	10.94	7.599-16	5.892-10	7.678+05	7.754+05
50.00	13.62	8.000-16	6.922-10	8.584+05	8.652+05
60.00	16.30	7.808-16	7.391-10	9.403+05	9.466+05
70.00	18.99	7.777-16	7.944-10	1.016+06	1.021+06
80.00	21.67	7.606-16	8.300-10	1.086+06	1.091+06
90.00	24.35	7.606-16	8.798-10	1.152+06	1.157+06
100.00	27.03	7.553-16	9.206-10	1.214+06	1.219+06
120.00	32.39	7.375-16	9.840-10	1.330+06	1.334+06
150.00	40.44	7.451-16	1.111-09	1.487+06	1.491+06
180.00	48.48	7.553-16	1.233-09	1.629+06	1.632+06
200.00	53.85	7.200-16	1.239-09	1.717+06	1.720+06
220.00	59.21	7.200-16	1.299-09	1.801+06	1.804+06
250.00	67.26	7.451-16	1.432-09	1.919+06	1.922+06
280.00	75.30	7.200-16	1.465-09	2.031+06	2.034+06
300.00	80.66	7.200-16	1.516-09	2.103+06	2.105+06
325.00	87.37	7.200-16	1.578-09	2.188+06	2.191+06
350.00	94.07	7.050-16	1.603-09	2.271+06	2.274+06
400.00	107.48	7.103-16	1.726-09	2.428+06	2.430+06
450.00	120.89	6.666-16	1.718-09	2.575+06	2.577+06
500.00	134.30	6.666-16	1.811-09	2.714+06	2.717+06
550.00	147.70	7.050-16	2.009-09	2.847+06	2.849+06
600.00	161.11	7.312-16	2.176-09	2.973+06	2.975+06
700.00	187.93	8.191-16	2.632-09	3.212+06	3.214+06
800.00	214.74	8.808-16	3.026-09	3.433+06	3.435+06
900.00	241.56	8.700-16	3.170-09	3.642+06	3.643+06
1000.00	268.37	8.653-16	3.323-09	3.839+06	3.840+06
1200.00	322.01	1.036-15	4.358-09	4.205+06	4.207+06
1500.00	402.45	1.067-15	5.018-09	4.702+06	4.703+06
1800.00	482.90	9.555-16	4.922-09	5.150+06	5.151+06
2000.00	536.53	9.555-16	5.188-09	5.429+06	5.430+06
2200.00	590.17	9.723-16	5.537-09	5.694+06	5.695+06
2500.00	670.61	1.111-15	6.744-09	6.070+06	6.071+06
3000.00	804.69	1.176-15	7.820-09	6.649+06	6.650+06
3500.00	938.77	1.176-15	8.447-09	7.182+06	7.182+06
4000.00	1072.85	1.194-15	9.168-09	7.678+06	7.678+06
4500.00	1206.93	1.200-15	9.773-09	8.143+06	8.144+06
5000.00	1341.01	1.200-15	1.030-08	8.584+06	8.584+06

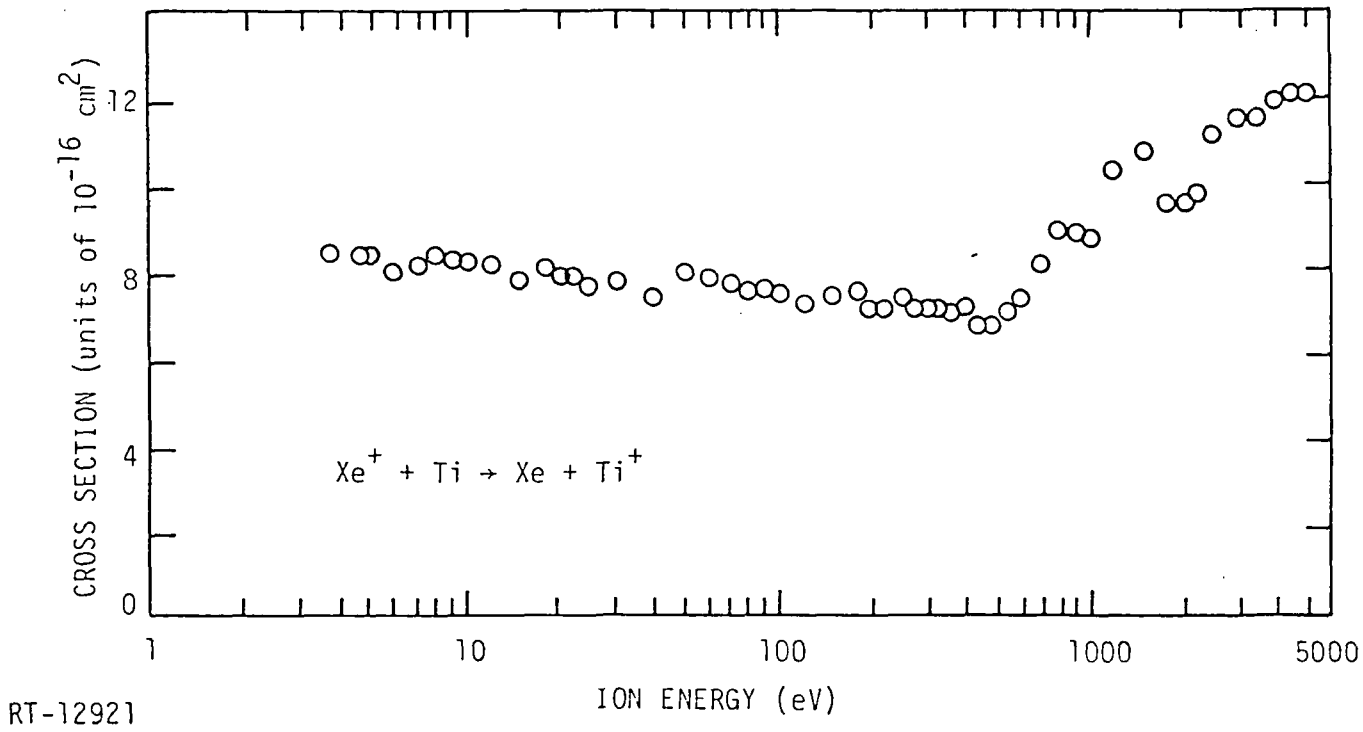

Figure 12. Cross section for the charge transfer process $Xe^+ + Ti \rightarrow Xe + Ti^+$ as a function of the ion energy

Table XI. Charge transfer cross sections between Hg^+ and Ta

ION MASS 200.0000,
NEUTRAL MASS 181.0000
NEUTRAL BEAM TEMPERATURE 3000.00
NEUTRAL VELOCITY 6.9923+04

ION LAB ENERGY (EV)	COLLISION ENERGY (EV)	CROSS SECTION (CM2)	RATE COEFFICIENT (CM3/SEC)	ION VELOCITY (CM/SEC)	RELATIVE VELOCITY (CM/SEC)
10.00	4.99	1.076-14	3.426-09	3.107+05	3.185+05
12.00	5.94	1.160-14	4.029-09	3.403+05	3.474+05
15.00	7.37	1.108-14	4.285-09	3.805+05	3.869+05
20.00	9.74	1.144-14	5.089-09	4.394+05	4.449+05
25.00	12.12	1.114-14	5.525-09	4.912+05	4.962+05
30.00	14.49	1.064-14	5.773-09	5.381+05	5.426+05
35.00	16.87	1.024-14	5.998-09	5.812+05	5.854+05
40.00	19.24	1.135-14	7.098-09	6.214+05	6.253+05
50.00	23.99	1.113-14	7.770-09	6.947+05	6.982+05
55.00	26.37	1.036-14	7.584-09	7.286+05	7.320+05
60.00	28.74	1.093-14	8.357-09	7.610+05	7.642+05
80.00	38.25	1.098-14	9.679-09	8.787+05	8.815+05
100.00	47.75	1.025-14	1.009-08	9.825+05	9.849+05
150.00	71.50	9.492-15	1.144-08	1.203+06	1.205+06
180.00	85.75	1.004-14	1.326-08	1.318+06	1.320+06
200.00	95.25	1.075-14	1.496-08	1.389+06	1.391+06
220.00	104.76	9.925-15	1.448-08	1.457+06	1.459+06
250.00	119.01	9.812-15	1.526-08	1.553+06	1.555+06
275.00	130.89	1.099-14	1.793-08	1.629+06	1.631+06
300.00	142.76	9.652-15	1.644-08	1.702+06	1.703+06
350.00	166.52	1.074-14	1.976-08	1.838+06	1.839+06
400.00	190.27	1.007-14	1.980-08	1.965+06	1.966+06
450.00	214.02	1.020-14	2.128-08	2.084+06	2.085+06
500.00	237.78	1.063-14	2.337-08	2.197+06	2.198+06
550.00	261.53	9.957-15	2.295-08	2.304+06	2.305+06
600.00	285.28	1.138-14	2.740-08	2.407+06	2.408+06
700.00	332.79	1.155-14	3.004-08	2.599+06	2.600+06
800.00	380.30	1.092-14	3.035-08	2.779+06	2.780+06
900.00	427.80	1.011-14	2.980-08	2.947+06	2.948+06
1000.00	475.31	1.149-14	3.571-08	3.107+06	3.108+06
1100.00	522.82	1.184-14	3.859-08	3.258+06	3.259+06
1200.00	570.33	1.149-14	3.912-08	3.403+06	3.404+06
1500.00	712.85	1.162-14	4.422-08	3.805+06	3.806+06
1800.00	855.37	1.154-14	4.812-08	4.168+06	4.169+06
2000.00	950.38	1.159-14	5.091-08	4.394+06	4.394+06
2200.00	1045.40	1.195-14	5.510-08	4.608+06	4.609+06
2500.00	1187.92	1.130-14	5.551-08	4.912+06	4.913+06
3000.00	1425.45	1.117-14	6.011-08	5.381+06	5.382+06
3500.00	1662.99	1.103-14	6.413-08	5.812+06	5.813+06
4000.00	1900.53	1.148-14	7.134-08	6.214+06	6.214+06
4500.00	2138.06	1.108-14	7.304-08	6.591+06	6.591+06
5000.00	2375.60	1.061-14	7.368-08	6.947+06	6.947+06
5500.00	2613.13	1.208-14	8.803-08	7.286+06	7.286+06

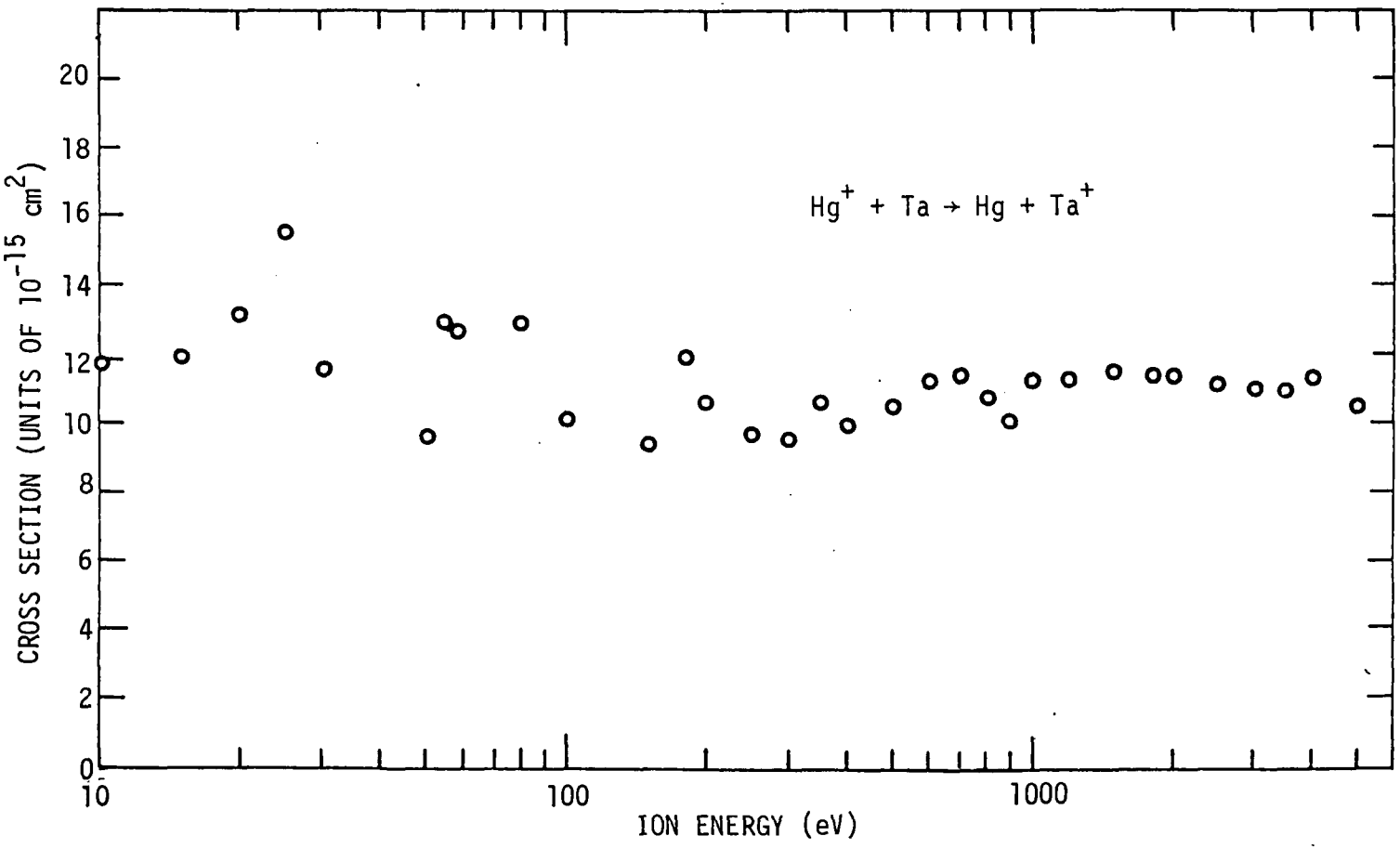

RT-14952

Figure 13. Charge transfer cross section for the reaction $Hg^+ + Ta \rightarrow Hg + Ta^+$ as a function of primary ion energy

3.6 CARBON

Data has been obtained for mercury ions in collision with carbon particles. All possible reactions are endothermic.

The stability of the beam of carbon particles formed by the e-beam heater was not as good as for tantalum, but was adequate for the measurements made here. Tests with several ions established that the carbon particle beam consisted primarily of C, C_2 and C_3 species with some indication of higher polymers. Examples of reactions used to identify the components of the carbon beam are

$$C^+ + C \rightarrow C + C^+$$

$$H_2^+ + C \rightarrow H_2 + C^+$$

$$H_2^+ + C_2 \rightarrow H_2 + C_2^+$$

$$H_2^+ + C_3 \rightarrow H_2 + C_3^+$$

$$H_2^+ + C_4 \rightarrow H_2 + C_4^+ \quad \text{very small signal}$$

$$H_2^+ + C_5 \rightarrow H_2 + C_5^+ \quad \text{indication of a signal}$$

The ionization potential of Hg is 10.44 eV which is less than that for carbon (11.26 eV) and the carbon polymers. As a consequence, no signals due to charge cross sections would be expected for collisions between Hg^+ and C, C_2 and C_3 (Reactions 12, 13, and 14) in the low energy regime. Experiments to determine if any measurable signals could be detected were carried out. For Reactions 12 and 13 no signals could in fact be detected over the energy range from 1 to 5000 eV. For Reaction 14, however, signals were seen in the energy range above 1000 eV.

In order to determine upper limits for the reaction of Hg^+ with C and C_2 and to establish the size of the cross section for Hg^+ reacting with C_3, it is necessary to know the beam density of each species. From our measurements of H_2^+ in collision with carbon particles, assuming equal charge transfer cross sections for all processes, we have been able to determine that C_3 is the largest component of the beam followed by C with C_2 being slightly smaller than C. Higher order polymers were much smaller. Because the cross section values are not known for H_2^+ in collision with C, C_2 and C_3, it was not possible to put the ratios on an absolute basis.

In order to get an idea of the ratio of the carbon species, we have used the results determined by Burns et al. (Ref. 12) for the ratio of C, C_2 and C_3 at 2500 K under non-equilibrium evaporation conditions. Our e-beam heater operated at similar temperatures and evaporation was taken to be non-equilibrium. The ratios obtained by Burns et al. were 1.0 to 1.0 to 1.6 for C to C_2 to C_3. These values are in agreement with our rough determination using H_2^+ charge transfer.

Using these ratios and the fact that the $C^+ + C$ symmetric charge transfer has been measured previously using merging beam techniques (Ref. 13), it was possible to put upper limits on the cross sections for Hg^+ charge transfer to C and C_2 and to give cross section values for Hg^+ in collision with C_3 above 800 eV. The cross section value used for normalization is $C^+ + C \rightarrow C + C^+$ equal to 3.6×10^{-15} cm^2 at 200 eV ion energy. The values obtained are displayed in Tables XII and XIII.

Table XII

Upper limits for the charge transfer cross sections between Hg^+ and C and C_2

Species	Ion Energy Range (eV)	Upper Limit on the Cross Section (cm^2)
C	1-5000	5.10×10^{-17}
C_2	1-5000	7.0×10^{-17}

Table XIII

Charge transfer cross sections between Hg^+ and C_3

Ion Energy (eV)	Cross Section (cm^2)
< 800	$< 4.0 \times 10^{-17}$
1000	2.4×10^{-16}
1500	3.7×10^{-16}
2000	1.3×10^{-16}
3000	4.7×10^{-16}
4000	4.9×10^{-16}
5000	5.1×10^{-16}

4. OPTICAL MEASUREMENT RESULTS AND DISCUSSION

Attempts were made to observe optical emissions from several of the charge transfer systems discussed in Section 3. In all cases, no optical signals that could be ascribed to the process under study could be identified. Where possible upper limits of cross sections for emission have been determined and are listed below.

Several reasons for the failure to observe radiation due to formation of excited product can be given. For example, the excited state may radiate to a number of different states such that the photons emitted due to any one process are below the detection limit of our apparatus. Further, our search for emission was limited to the range from 400 to 700 nm and the wavelength of the radiation may have been outside this range. The excited species formed in the collision may be in a metastable state and not radiate before they travel out of the observation region of our apparatus. Another possibility is that the excess energy in the reaction does not go into formation of excited product states at all. That is, the excess energy in the collision manifests itself in another manner such as translational motion of the products.

Some general evidence exists that cross sections for emission of radiation from products of charge neutral collisions are generally considerably smaller than the total reaction cross sections (Ref. 14). The results obtained here seem to support this statement.

Upper limits for the processes investigated are given in Table XIV. The values were determined by establishing the sensitivity of the optical apparatus using the known cross section for a system with known optical emissions, namely,

$$\begin{array}{l} He^+ + N_2 \rightarrow He + N_2^+ \\ \qquad\qquad\quad \downarrow \\ \qquad\qquad\quad \rightarrow N_2^+ + h\nu \end{array} .$$

Here $h\nu$ is the 3914 Å 0-0 transition of the second negative band system for N_2^+. The cross section for this process is known to be 1.6×10^{-18} cm^2 for 300 eV

He^+ impinging on N_2 (Ref. 15). Using the optical signal generated by this process for a known N_2 beam density and He^+ current, it is possible to get upper limits for the processes involving the metal atoms if the metal atom beam density and ion currents are known.

Table XIV

Upper limits on the cross sections for emission of radiation from metallic species

Process	Upper Limit (cm^2)
$Hg^+ + Fe \rightarrow Hg + Fe^+$	2×10^{-16}
$Xe^+ + Fe \rightarrow Xe + Fe^+$	1×10^{-16}
$Hg^+ + Mo \rightarrow Hg + Mo^+$	1×10^{-16}
$Xe^+ + Mo \rightarrow Xe + Mo^+$	2×10^{-16}

5. SUMMARY

Proposed space missions using electric propulsion will probably use thrusters with specific impulse in the range of 2000 to 5000 seconds. This range corresponds to beam ion velocities of 2×10^6 to 5×10^6 cm/sec.

Table XV has been prepared to enable comparison of charge transfer cross section data for various reactions at constant ion velocity. Constant ion velocity is chosen because many space missions are designed using constant specific impulse thrusters. Cross section data, obtained from the literature is also included in Table XV for each ion reacting with its neutral atom because such reactions will produce the major quantity of charge transfer ions.

As can be seen in Table XV, there are, as expected, relatively small changes in cross section values for a given reaction within the range of ion velocity presented. Hg^+ charge transfer with Ta or Ti neutral atoms is seen to be of the same order of magnitude as for the charge transfer cross section with neutral Hg. The metal atoms, Mo, Al and Fe, however, have an order of magnitude lower cross section, and carbon atoms are two orders of magnitude lower. Thus, if any condensible metal atoms must be present in a thruster Hg^+ ion beam, the lowest level of spacecraft contamination would accrue if these atoms would be C, Fe, Al or Mo, rather than Ta or Ti.

Few measurements of charge transfer between atomic species other than the rare gases exist. The studies detailed above therefore have interest beyond those of the NASA ion thruster program.

The metallic species studied have, for the most part, many excited states in both their neutral and ionic forms. The availability of these states for the absorption of the excess energy of reaction (for exothermic processes) makes near resonant processes possible. Many past studies done on simpler systems involving both atomic and molecular species have indicated that large cross sections ($> 5 \times 10^{-15}$ cm^2) exhibiting little structure are found for cases of

Table XV. Comparison of cross sections at constant ion velocity with various atoms

a. Ion velocity, 2×10^6 cm/sec

Ion	Ion Energy (eV)	Ta	Ti	Mo	Al	Fe	C_3	C_2	C	Hg[16]	Xe[16]	Cs[17]
Hg^+	415	100	30	10	4	6	<0.4	<0.7	<0.5	85	--	--
Xe^+	270	--	7	6	4	3	--	--	--	--	40	--
Cs^+	275	--	--	--	<0.05	<0.07	--	--	--	--	--	320

b. Ion velocity, 3×10^{16} cm/sec

Ion	Ion Energy (eV)	Ta	Ti	Mo	Al	Fe	C_3	C_2	C	Hg[16]	Xe[16]	Cs[17]
Hg^+	930	100	34	7	5	4	2	<0.7	<0.5	75	--	--
Xe^+	610	--	7	5	2	3	--	--	--	--	35	--
Cs^+	620	--	--	--	<0.03	<0.04	--	--	--	--	--	300

c. Ion velocity, 5×10^6 cm/sec

Ion	Ion Energy (eV)	Ta	Ti	Mo	Al	Fe	C_3	C_2	C	Hg[16]	Xe[16]	Cs[17]
Hg^+	2590	120	38	7	6	4	3	<0.7	<0.5	60	--	--
Xe^+	1700	--	10	5	3	3	--	--	--	--	30	--
Cs^+	1720	--	--	--	<0.06	<0.1	--	--	--	--	--	250

near or accidental resonance. (By accidental resonance, it is meant that there was at least one set of energy levels of the product particles such that the total excess energy in the process could be exactly absorbed into internal energy.) Most of the cross sections measured here are considerably smaller than the value given above.

A major accomplishment of the program was the development of neutral beam sources for the metals studied. Considerable effort had to be expended in some cases to meet the requirements of the program. This was particularly true in the development of beam sources for Mo, Ta and C. In general, the development of the new beam sources was merely the application of known technology to a problem. Some surprises were encountered however, particularly for titanium where an indication was obtained that there may be considerable error in the published value of the vapor pressure at temperatures near the melting point.

REFERENCES

1. John F. Staggs, William P. Gula and William R. Kerslake, "Distribution of Neutral Atoms and Charge-Exchange Ions Downstream of an Ion Thruster," J. Spacecraft 5, 159 (1968).

2. J. A. Rutherford, R. F. Mathis, B. R. Turner, and D. A. Vroom, "Formation of Magnesium Ions by Charge Transfer," J. Chem. Phys. 55, 3875 (1971).

3. R. F. Stebbings, B. R. Turner, and J. A. Rutherford, "Low-Energy Collisions Between Some Atmospheric Ions and Neutral Particles," J. Geophys. Res. 71, 771 (1966).

4. B. R. Turner, J. A. Rutherford, and R. F. Stebbings, "Charge Transfer Reactions of Nitric Oxide and Atomic and Molecular Ions of Oxygen and Nitrogen," J. Geophys. Res. 71, 4521 (1966).

5. M. G. Inghram and Q. J. Hayden, "Mass Spectrometry," Nuclear Science Series Report Number 14, National Academy of Sciences, Washington, D. C., 1954.

6. M. Knudsen, "Kinetic Theory of Gases," Methuen's Monographs on Physics Subjects, 3rd ed., Methuen & Co., Ltd., London, 1950.

7. R. E. Honig, "Vapor Pressure Data for the Solid and Liquid Elements," RCA Review 23, 567 (1962).

8. J. A. Rutherford and D. A. Vroom, "Formation of Iron Ions by Charge Transfer," J. Chem. Phys. 57, 3091 (1972).

9. R. T. Sanderson, "Chemical Periodicity," p. 119, Rienhold Publishing Corp., New York, 1960.

10. J. A. Rutherford, R. F. Mathis, B. R. Turner and D. A. Vroom, "Formation of Sodium Ions by Charge Transfer," J. Chem. Phys. 56, 4654 (1972).

11. J. A. Rutherford, R. F. Mathis, B. R. Turner and D. A. Vroom, "Formation of Calcium Ions by Charge Transfer," J. Chem. Phys. 57, 3087 (1972).

12. R. P. Burns, A. J. Jason, and M. G. Inghram, "Evaporation Coefficient of Graphite, J. Chem. Phys. 40, 1161 (1964).

13. V. A. Belyaev, B. G. Brezhnev and E. M. Eraston, "Resonant Charge Transfer of Low-Energy Carbon and Nitrogen Ions," Soviet Physics JETP 27, 924 (1968).

14. See, for example: J. Appell, D. Brandt and Ch. Ottenger, Chem. Phys. Letters 33, 131 (1975); C. R. Dickson and R. N. Zare, Chem. Phys. 7, 361 (1975); M. J. Haugh and J. H. Birely, J. Chem. Phys. 60, 264 (1974); and D. J. Wren and M. Menzinger, Chem. Phys. Letters 25, 378 (1974).

15. B. R. Turner and J. A. Rutherford, "Electronic and Ionic Reactions in Atmospheric Gases," Yearly Technical Summary Report, Gulf General Atomic Report No. GA 9827, Jan. 28, 1970.

16. Taken from "Electronic and Ionic Impact Phenomena, Vol. IV, p. 2772, by H. S. W. Massey and H. B. Gilbody, Oxford (1974).

17. L. L. Marino, A. C. H. Smith, and E. Caplinger, "Charge Transfer Between Positive Cesium Ions and Cesium Atoms," Phys. Rev. 128, 2243 (1962).